UNIVERSITAT DE BARCELONA

Facultat de Matemàtiques
i Informàtica

GRAU DE MATEMÀTIQUES

Treball final de grau

Richness of the Dynamics at a Shilnikov Bifurcation

Autor: Oriol Tellols Asensi

Director: Dr. Arturo Vieiro Yanes
Realitzat a: Departament de Matemàtiques i Informàtica

Barcelona, 20 de juny de 2021

Acknowledgements

This Final Degree Thesis has been possible thanks to the support, knowledge and motivation received from many different people.

I want to thank all the professors of the Faculty of Mathematics and Computer Science of the University of Barcelona who have accompanied me during my studies in the Bachelor's Degree in Mathematics and that have provided me with a lot of valuable knowledge.

Special thanks go to Arturo Vieiro Yanes, my project supervisor, for motivating me to pursue my path in the field of Dynamical Systems, for his suggestions, and for helping me make this project unique.

Finally, I want to thank my parents and my sister Dolça for their unconditional support.

Aquest Treball de Final de Grau ha estat possible gràcies al suport i la motivació rebudes per part de moltes persones.

Voldria agrair a tot el professorat de la Facultat de Matemàtiques i Informàtica de la Universitat de Barcelona que m'ha acompanyat durant els meus estudis del Grau de Matemàtiques i que m'ha aportat tants coneixements.

Especialment, el meu agraïment va dirigit a Arturo Viero Yanes, el meu director del projecte, per motivar-me a seguir el camí del camp dels Sistemes Dinàmics, pels seus suggeriments, i per ajudar-me a fer que aquest projecte sigui únic.

Finalment, vull agrair als meus pares i a la meva germana Dolça tot el seu suport incondicional.

Abstract

In this work, we study the dynamics exhibited in 3−dimensional parametric continuous dynamical systems containing a homoclinic orbit to a saddle-focus equilibrium. This setting gives rise to the Shilnikov bifurcation, which can be studied using an appropriate Poincaré section that reduces the original system into a discrete 2−dimensional one. The bifurcation presents various cases, each showing rich and different dynamics. The Shilnikov Theorem describes one of the possible scenarios. This case follows from a careful analysis of a suitable return map that shows that dynamics in some regions is equivalent to the one of the horseshoe map. To illustrate properties and scenarios appearing at the bifurcation, we derive a family of systems with the desired properties and investigate them numerically.

En aquest treball, estudiem la dinàmica exposada en sistemes dinàmics paramètrics continus 3−dimensionals que contenen una òrbita homoclínica a un equilibri sella-focus. Aquesta configuració dóna lloc a la bifurcació de Shilnikov, que pot ser estudiada utilitzant una secció de Poincaré adequada que redueix el sistema original a un discret 2−dimensional. La bifurcació presenta diversos casos, cadascun mostrant una dinàmica rica i diferent. El Teorema de Shilnikov descriu un dels possibles escenaris. Això segueix d'una anàlisi acurada d'una aplicació de retorn adequada que mostra que la dinàmica en algunes regions és equivalent a la de la ferradura de Smale. Per tal d'il·lustrar propietats i escenaris que aparèixen a la bifurcació, derivem una família de sistemes que tenen les propietats desitjades i els investiguem numericament.

2020 Mathematics Subject Classification. 37C10, 37C29, 37D45, 37G20

Contents

Introduction

Classical problems like those from celestial mechanics, which appeared naturally to understand the motions of the bodies of the solar system, have drawn the interest of scientists for many centuries. The study of these problems lead to the dynamical systems theory and show the difficulties of nonlinear dynamics.

Henri Poincaré was a pioneer, and his work in the late nineteenth century paired analysis and geometry, giving a new qualitative approach. This perspective raised further questions, and other branches in the theory of dynamical systems emerged. One of those is bifurcation theory, that is, the study of qualitative changes in the phase space as the parameters of a system are varied. A formalization of those ideas to describe changes in the structure of the phase space was first given by Andronov and Pontryagin in 1937 with the introduction of rough systems. This concept evolved into the notion of structural stability, which is a weaker type of rough system but more appropriate from the mathematical point of view to describe the appearance of bifurcations formally.

In this work, we study the Shilnikov bifurcation, which stands for the global bifurcation arising from the destruction of a homoclinic orbit to a saddle-focus equilibrium. The analysis of the different dynamics in this setting requires various techniques in dynamical systems such as the construction of Poincaré maps, the search for topologically conjugated systems to an original one that facilitates its study, and the appearance of a new robust type of chaos. Although the Shilnikov bifurcation scenario presents rich dynamics and is worth studying by itself, many mathematical models arising, for example, in electronics or neuroscience exhibit similar behaviours that can be understood from the theoretical approach of this topic. See the introduction of Chapter 5 for further comments and references.

The main objective in this work is to thoroughly understand the dynamics in a tubular neighbourhood of the homoclinic orbit to a saddle-focus at a Shilnikov bifurcation. We do all of this in the context of $3-$dimensional parametric continuous

dynamical systems that tend to exhibit complicated dynamics, and in which many of the tools and results used in lower dimensions, like the Poincaré-Bendixson Theorem, are no longer available.

In Chapter 1 we introduce the elementary definitions and notation for this work. Then, we describe some properties of the invariant manifolds of a hyperbolic equilibrium stating the Stable Manifold Theorem. With that information, we justify that homoclinic orbits to hyperbolic equilibrium are structurally unstable and hence cause the appearance of a bifurcation. The last subsection introduces the split function, which gives the relative position between the invariant manifolds of a hyperbolic equilibrium and formalizes some hypotheses used later.

In Chapter 2 we consider a $3-$dimensional parametric continuous dynamical system presenting a Shilnikov bifurcation, and we introduce a Poincaré section to reduce the original system into a discrete $2-$dimensional one. The construction of this Poincaré map requires an exhaustive study of the local flow around the saddle-focus, and the iteration of this discrete map gives rise to two different scenarios presenting independent dynamics depending on the sign of the saddle value. The case $\sigma < 0$ is studied here and exhibits the appearance of a stable limit cycle, which the Banach Fixed Point Theorem justifies.

Chapter 3 is devoted to the study of the horseshoe map, a $2-$dimensional discrete system presenting chaotic behaviour. First, we define it and show some of its main properties. Then, we give conditions determining topological conjugacy with the horseshoe map. In Chapter 4 we check the satisfaction of the conditions applied to the Poincaré map defined in Chapter 2 to prove the Shilnikov Theorem that describes the dynamics of a Shilnikov system in a tubular neighbourhood of the homoclinic orbit to the saddle-focus in the case $\sigma > 0$.

Finally, in Chapter 5 we derive a family of systems containing a homoclinic orbit to a hyperbolic equilibrium using recent techniques. This allows us to illustrate the bifurcation scenarios when $\sigma > 0$ and when $\sigma < 0$ making few modifications on the vector field determining one of such systems. Using those systems, we implemented the Taylor method to find numerical solutions of ODEs and illustrate the homoclinic bifurcation when $\sigma > 0$. Additionally, we implemented a method to determine the exact type of stability of the limit cycle emerging when $\sigma < 0$ using a Poincaré map computed numerically.

Chapter 1

Homoclinic phenomena

This chapter aims to study the appearance of bifurcations in systems containing homoclinic orbits to hyperbolic equilibria. In particular, we will use the general setting discussed here in the description of the Shilnikov bifurcation in Chapter 2, where we see that a homoclinic configuration of a concrete type leads to a richness of dynamics nearby. The contents here are mainly inspired in these references: [Kuz13], [GH13], [HSD12].

1.1 Preliminary definitions

This section sets the notation that will be used throughout the manuscript. We start by recalling that a dynamical system is a triplet (T, X, φ), where T is the time set, $X \subseteq \mathbb{R}^n$, $n \in \mathbb{N}$ is the state space and $\varphi : \Omega \subseteq T \times X \to X$ is the evolution law satisfying:

- $\varphi(0, \cdot) = Id_X$
- $\varphi(t + s, x) = \varphi(t, \varphi(s, x))$

The time interval of $x \in X$ is $I(x) = \{t \in T : (t, \varphi(t, x)) \in \Omega\}$. The last condition must be satisfied for every $t, s \in T$ such that $\{s, t + s\} \subseteq I(x)$ and $t \in I(\varphi(s, x))$.

We are interested in continuous and discrete dynamical systems, for which either $T = \mathbb{R}$ or $T = \mathbb{Z}$. In the discrete case, the evolution law $\varphi(t, x)$ is given by a continuous function $f : X \to X$ such that $\varphi(t, x) = f^t(x)$, where f^t is the result of composing f with itself t times. Indeed, all the discrete systems that we deal with in this project are defined by a smooth bijective function.

From the basic theory on differential equations, we know that if $\dot{x} = f(x)$ is an $n-$dimensional autonomous differential equation, where $f : U \to \mathbb{R}^n$, $U \subseteq \mathbb{R}^n$ open set, the evolution law φ defines a flow provided existence and uniqueness of solutions of Cauchy problems. This holds for example, whenever $f \in \mathcal{C}^r$ with $r \geq 1$. When not specified, the open set will be $U = \mathbb{R}^n$, which is not a restrictive assumption, because we are only interested in local or semi-global (around a homoclinic orbit, see definition later) properties. Also, we shall assume that solutions can be extended to all times, that is, $I(x) = \mathbb{R}, \forall x \in U$. This is neither a restrictive assumption, since completeness can be achieved by multiplying the vector field by an integrating factor.

Let us recall some common definitions in dynamical systems.

Definition 1.1. The orbit starting at x_0 is $Or(x_0) = \{\varphi(t, x_0) : t \in I(x_0)\}$.

Here we define the $\alpha - limit$ and $\omega - limit$ of a point that determine the asymptotic behaviour of its orbit.

Definition 1.2. Let $f : V \to \mathbb{R}$ be a $\mathcal{C}^r$ vector field on the open set V for $r \geq 1$ and let $\varphi : \mathcal{R} \times V \to V$ be the flux of the dynamical system $\dot{x} = f(x)$. Then the $\alpha - limit$ and the $\omega - limit$ of $x \in V$ are:

$$\alpha(x) = \{y \in V : \exists (t_k)_k \text{ such that } \lim_{k\to\infty} t_k = -\infty \text{ and } \lim_{k\to\infty} \varphi(t_k, x) = y\}$$

$$\omega(x) = \{y \in V : \exists (t_k)_k \text{ such that } \lim_{k\to\infty} t_k = +\infty \text{ and } \lim_{k\to\infty} \varphi(t_k, x) = y\}$$

The definition of $\alpha - limit$ and $\omega - limit$ varies slightly for discrete systems, taking into account that $T = \mathbb{Z}$ and that the evolution process is given by the iterates of f.

Given an evolution law $\varphi : \mathbb{R} \times U \to U$ and two points $x_0, x_1 \in U$, one can define an equivalence relation $\mathcal{R}$ defined by $x_0 \mathcal{R} x_1$ if and only if $x_0 \in Or(x_1)$. Therefore, we can consider the quotient set $U/\mathcal{R}$. Additionally, $x_0 \mathcal{R} x_1$ implies that $Or(x_0) = Or(x_1)$, which lets us set an order relation defined by $x_0 \leq x_1$ if and only if there exists $t \geq 0$ such that $x_1 = \varphi(t, x_0)$.

Definition 1.3. The phase portrait of a dynamical system is the partition of the phase space into orbits.

The interest of the qualitative theory of ordinary differential equations and, in general, of dynamical systems is describing the different topologies of the orbits to obtain a geometrical description of the phase space structure.

Definition 1.4. A point $x \in X$ is called an equilibrium if $\varphi(t, x) = x, \forall t \in \mathbb{R}$.

Definition 1.5. An invariant set is a subset $S \subset X$ such that $\varphi(t, x) \in S, \forall x \in S$ and $\forall t \in \mathbb{R}$.

To introduce the concept of bifurcation, we need an equivalence relation between dynamical systems. The following definitions present the concepts of topological equivalence and of topological conjugacy, the second demanding a stronger condition than the first. Both concepts will play a key role in this work.

Definition 1.6. Two dynamical systems $\{T, \mathbb{R}^n, \varphi\}$ and $\{T, \mathbb{R}^n, \phi\}$, are topologically equivalent if there exists a homeomorphism $h : \mathbb{R}^n \to \mathbb{R}^n$ mapping orbits of the first system onto orbits of the second system and preserving the orientation of time. The phase portraits of two topologically equivalent dynamical systems are also called topologically equivalent.

Definition 1.7. Two continuous functions $f : X \to X$ and $g : Y \to Y$ are topologically conjugated if there exists a homeomorphism $h : X \to Y$ such that $h \circ f = g \circ h$.

Definition 1.8. Let $\dot{x} = f(x, \gamma)$ be a parametric dynamical system, where $\gamma \in \mathbb{R}^p$ with $p \geq 1$ and f depends smoothly with respect to both, x and γ. A bifurcation occurs when a topological nonequivalent phase portrait appears as the parameters pass through a critical value.

There are different types of bifurcations. A general and classical classification distinguishes between those bifurcations that depend on local properties around a fixed point and those bifurcations that depend on global properties of the phase space. In the context of continuous systems, the first type includes the classical saddle-node, transcritical, pitchfork and Hopf bifurcations, among others (see [HSD12]). The second type of bifurcations are typically related to a change of the topology due to the relative position of the stable and/or the unstable manifolds associated with hyperbolic objects that extend along phase space and interact between others giving rise to homoclinic or heteroclinic bifurcations.

Another concept that will be useful is the concept of structural stability. To introduce it, we need to define the $\mathcal{C}^1$ distance between dynamical systems.

Definition 1.9. Let $\|\cdot\|$ be a vector and matrix norm in $\mathbb{R}^n$ and consider two dynamical systems $\dot{x} = f(x)$ and $\dot{x} = g(x)$, with f and g smooth functions. Their distance in a closed region $V \subset \mathbb{R}^n$ is:

$$d = \sup_{x \in V} \{\|f(x) - g(x)\| + \|Df(x) - Dg(x)\|\}$$

We say that the systems are $\mathcal{C}^1$-close if their $\mathcal{C}^1$ distance is lower than ϵ for a given $\epsilon > 0$.

This definition of distance ensures that close systems have similar orbits and equilibria because both the vector fields and their derivatives must be similar.

Definition 1.10. A dynamical system $\dot{x} = f(x)$ with f smooth function, defined in a region $D \subset \mathbb{R}^n$ is structurally stable in a region $D_0 \subset D$ if for any sufficiently $\mathcal{C}^1$-*close* system $\dot{x} = g(x)$ with g smooth function defined in D, there exist regions $U, V \subset D$ such that $D_0 \subset U$ and $\dot{x} = f(x)$ is topologically equivalent in U to $\dot{x} = g(x)$ in V.

1.2 Homoclinic bifurcations

Throughout this section we will consider a system of autonomous ordinary differential equations $\dot{x} = f(x)$, with $f : \mathbb{R}^n \to \mathbb{R}^n$ a smooth function. The aim is to show that qualitative changes in the topology of the phase space may occur under the existence of a homoclinic orbit to a hyperbolic fixed point. Moreover, we will introduce additional tools to describe homoclinic bifurcations.

1.2.1 Invariant sets of a hyperbolic point

Homoclinic orbits to a hyperbolic point x_0 are closely related to the invariant sets of x_0. To better understand this connection, we need to review the definitions and properties of the elements involved.

Definition 1.11. An equilibrium x_0 is hyperbolic if $Re(\lambda) \neq 0, \forall \lambda \in Spec(Df(x_0))$.

We recall that if the vector field f is defined on $\mathbb{R}^2$ and x_0 is a hyperbolic fixed point of f such that $Spec(Df(x_0)) = \{\lambda_1, \lambda_2\}$, then x_0 is classified according to the following criteria:

- If $\lambda_1, \lambda_2 \in \mathbb{R}$, $\lambda_1 \neq \lambda_2$ and $\lambda_1\lambda_2 > 0$, then x_0 is a node. The node is stable if $\lambda_1, \lambda_2 < 0$ and unstable if $\lambda_1, \lambda_2 > 0$.
- If $\lambda_1, \lambda_2 \in \mathbb{R}$, $\lambda_1 \neq \lambda_2$ and $\lambda_1\lambda_2 < 0$, then x_0 is a saddle.
- If $\lambda_1 = \overline{\lambda_2} = \alpha + i\beta$ with $\beta \neq 0$, then x_0 is a focus. The focus is stable if $\alpha < 0$ and unstable if $\alpha > 0$.

If the vector field f is defined on $\mathbb{R}^3$ and it has a hyperbolic fixed point $x_0 \in \mathbb{R}^3$ such that $Spec(Df(x_0)) = \{\lambda, \alpha + \beta i, \alpha - \beta i\}$ with $\lambda, \alpha, \beta \in \mathbb{R}$ and $\lambda\alpha < 0$, then x_0 is a saddle-focus. This type of hyperbolic equilibrium will be of special interest when studying the Shilnikov bifurcation in Chapter 2.

Definition 1.12. An orbit Γ_0 starting at a point $x \in \mathbb{R}^n$ is homoclinic to an equilibrium point x_0 if $\lim_{t\to\pm\infty} \varphi(t,x) = x_0$. Therefore, the limit sets of a homoclinic orbit are totally determined because $\alpha(x) = \omega(x) = x_0, \forall x \in \Gamma_0$.

Definition 1.13. Let $x_0 \in \mathbb{R}^n$ be an equilibrium. The stable manifold of x_0 is $W_S^s(x_0) = \{x \in \mathbb{R}^n : \varphi(t,x) \to x_0 \text{ as } t \to \infty\}$. Similarly, the unstable manifold of x_0 is $W_S^u(x_0) = \{x \in \mathbb{R}^n : \varphi(t,x) \to x_0 \text{ as } t \to -\infty\}$.

The Stable Manifold Theorem gives more specific properties on these sets under the hypothesis of x_0 being hyperbolic. Indeed, it states that the sets are immersed manifolds in a neighbourhood of x_0. The statement given here is inspired by [Kuz13].

Theorem 1.14. (Stable Manifold Theorem) Let $f : \mathbb{R}^n \to \mathbb{R}^n$ be a $\mathcal{C}^r$ vector field for $r \geq 1$ containing a hyperbolic equilibrium x_0. Let E^s and E^u be the eigenspaces of $\sigma^s = \{\lambda \in Spec(Df(x_0)) : Re(\lambda) < 0\}$ and $\sigma^u = \{\lambda \in Spec(Df(x_0)) : Re(\lambda) > 0\}$. Then, there exist a small neighbourhood U of x_0 such that $W^s(x_0) = U \cap W_S^s(x_0)$ and $W^u(x_0) = U \cap W_S^u(x_0)$ are $\mathcal{C}^r$ manifolds tangent to E^s and E^u at x_0.

In general, if x_0 is an equilibrium of f, one has that $\mathbb{R}^n = E^s \oplus E^u \oplus E^c$, where E^c is the eigenspace of $\sigma^c = \{\lambda \in Spec(Df(x_0)) : Re(\lambda) = 0\}$. Hence, if x_0 is hyperbolic, then $\sigma^c = \emptyset$ and $\mathbb{R}^n = E^s \oplus E^u$. Consequently, if Γ_0 is a homoclinic orbit to a hyperbolic equilibrium x_0, then $\Gamma_0 \subseteq W^s(x_0) \cap W^u(x_0)$.

1.2.2 Homoclinic orbits to hyperbolic points

Consider a system $\dot{x} = f(x,\gamma)$, where $\gamma \in \mathbb{R}^p,\ p \geq 1$ is a parameter. Assume that for $\gamma = \gamma_0$, the system has a homoclinic orbit to a hyperbolic equilibrium point x_0. Our goal in this section is to show that for γ close to γ_0, the system has some bifurcations in a neighbourhood of the homoclinic orbit.

Let us define a few elementary notions from transversality theory that are needed to prove the most significant result in this section.

Definition 1.15. Let M, N be submanifolds of a differentiable manifold Z. M and N are transverse ($M \pitchfork N$) if $\forall p \in M \cap N$,

$$T_pM + T_pN = T_pZ$$

where T_pM is the tangent space of the manifold M at the point p.

It is known that transversality is a generic property, which means that if M, N are two transverse manifolds and they are slightly deformed, the resulting manifolds M' and N' are also transverse. For further details and proofs on the genericity of the transversality between manifolds, see [Gre15]. In the following, if M, N are two non-transverse manifolds, we will only consider generic perturbations such that the resulting manifolds M' and N' are either transverse or satisfy that $M' \cap N' = \emptyset$.

When a continuous system possesses a homoclinic connection to a hyperbolic fixed point, the stable and unstable invariant manifolds of this point intersect in a non-transversal way along the homoclinic orbit. The following result asserts that having a homoclinic orbit to a hyperbolic point is a non-generic property, meaning that, under a generic perturbation, the perturbed stable and unstable invariant manifolds of the hyperbolic fixed point do not intersect.

Proposition 1.16. A homoclinic orbit to a hyperbolic equilibrium of $\dot{x} = f(x)$ is structurally unstable.

Proof. See section A.1 in Appendix A. □

From now on, we will be considering parametric systems $\dot{x} = f(x, \gamma) = f_\gamma(x)$ with $f : \mathbb{R}^3 \times \mathbb{R} \to \mathbb{R}^3$ a smooth function with respect to x and γ, containing a homoclinic orbit Γ_0 to a saddle-focus equilibrium x_0 for $\gamma = \gamma_0$ and such that the only real eigenvalue of $Df_{\gamma_0}(x_0)$ is $\lambda > 0$.

A dynamical system is structurally stable in a sufficiently small neighbourhood of a hyperbolic equilibrium point. Therefore, any system $f_{\gamma_1}(x)$ sufficiently $\mathcal{C}^1 - close$ to $f_{\gamma_0}(x)$ has a saddle-focus equilibrium near x_0, and its local stable and unstable manifolds are close to the local stable and unstable manifolds of x_0. Additionally, we know that by Prop 1.16, for almost all values γ_1 of the parameter γ close enough to γ_0, the system $f_{\gamma_1}(x)$ does not have a homoclinic orbit to the saddle-focus. Further details on the definition of generic property in a function space will be given in subsection 1.2.3 after the introduction of the split function.

In particular, the systems $\dot{x} = f(x, \gamma_0)$ and $\dot{x} = f(x, \gamma_1)$ are not topologically equivalent in a region around the homoclinic orbit, hence a bifurcation occurs with critical value γ_0. These bifurcations occurring around a homoclinic orbit to a hyperbolic equilibrium are said to be homoclinic bifurcations, and Shilnikov bifurcation is a particular case of those.

Definition 1.17. A homoclinic bifurcation to a saddle-focus equilibrium in $\mathbb{R}^3$ is called a Shilnikov bifurcation. Parametric systems containing a homoclinic orbit to a saddle-focus for a particular parameter value will be referred to as Shilnikov systems.

1.2.3 The split function

Since for parameters near γ_0 the invariant manifolds do not intersect, it is natural to define a split function that gives the relative position between them. This will be used in Chapter 2. The usefulness of the split function to the study of homoclinic bifurcations is considered in [Kuz13].

The split function is constructed using a Poincaré section.

Definition 1.18. A Poincaré section of f is a regular local hypersurface $\Sigma \subset \mathbb{R}^n$ transverse to the line through x with direction $f(x), \forall x \in \Sigma$. If Σ is a Poincaré section and we assume that the system has some global recurrent property so that the dynamics returns back to Σ, then one can define the first return map $g : \Sigma \to \Sigma$ which is usually called the Poincaré map associated to Σ.

The construction of the split function is quite intuitive in $\mathbb{R}^2$ and can be easily extended to $\mathbb{R}^3$. To get started, consider the system $\dot{x} = f(x, \gamma) = f_\gamma(x)$ where $f : \mathbb{R}^2 \times \mathbb{R} \to \mathbb{R}^2$ is a smooth vector field that contains a homoclinic orbit Γ_0 to a saddle point x_0 for $\gamma = \gamma_0$. The next steps lead to the definition of the split function:

- Let W^s and W^u be the stable and unstable manifolds of x_0 respectively, and take a point $x_1 \in \Gamma_0 \subset W^s \cap W^u$.
- Since $f(x_1) \neq 0$, there exists a one-dimensional Poincaré section Σ of f_{γ_0} such that $x_1 \in \Sigma$.
- Let γ_1 be a parameter value close to γ_0 and let W_1^s, W_1^u be the stable and the unstable manifolds of the saddle of the system $f_{\gamma_1}(x)$.
- Introduce the arc-length coordinate ξ in Σ such that the point $\Sigma \cap W_1^s$ corresponds to $\xi = 0$. Denote as $\xi^u_{\gamma_1}$ the value of ξ at the point $\Sigma \cap W_1^u$.

The split function in $\mathbb{R}^2$ is $\rho : X \to \mathbb{R}$ defined by $\rho(\gamma) = \xi^u_\gamma$, where $X \subseteq \mathbb{R}$ is a neighbourhood of γ_0 and ξ^u_γ is defined as specified above. Figure 1.1 illustrates the invariant manifolds and the Poincaré section in a neighbourhood of the saddle point for different values of ρ.

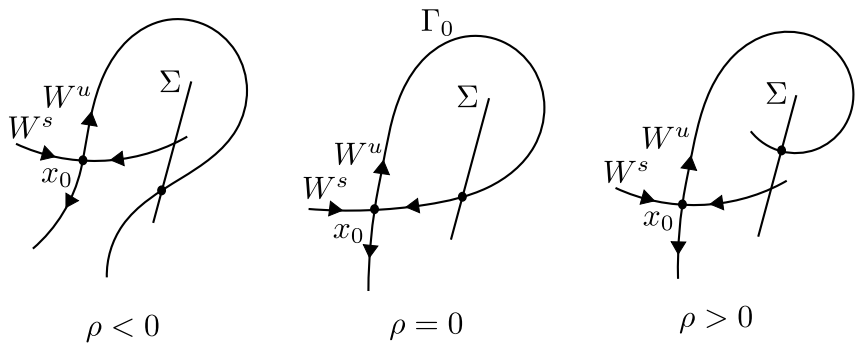

Figure 1.1: Different values of the split function in $\mathbb{R}^2$.

For a hyperbolic equilibrium $x_0 \in \mathbb{R}^3$ such that $dim(W^u(x_0)) = 1$ and $dim(W^s(x_0)) = 2$, the split function in $\mathbb{R}^3$ is built in the same way but now Σ is a two-dimensional Poincaré section with coordinates (ξ, μ) such that $\Sigma \restriction_{\xi=0} = \Sigma \cap W^s$. In this case, the split function $\rho : X \to \mathbb{R}$ is defined by $\rho(\gamma) = \xi_1^u$, where $(\xi_1^u, \mu_1^u) = \Sigma \cap W_1^u$. Notice that $\rho(\gamma) = 0$ if and only if $f_\gamma(x)$ has a homoclinic orbit $\Gamma_0 \subseteq W^s \cap W^u$, therefore $\rho(\gamma) = 0$ is a condition determining a homoclinic bifurcation in $\mathbb{R}^3$ with critical value γ_0.

In Chapter 2 it will be assumed that if $\rho(\gamma_0) = 0$, then $\rho'(\gamma_0) \neq 0$. This assumption guarantees that there is a change in the sign of $\rho(\gamma)$ as γ is varied strictly monotonically crossing γ_0. In other words, the unstable manifold goes from being below the stable manifold to being above or vice versa.

We end up this chapter with a technical remark concerning the non-generic property of homoclinic orbits to hyperbolic points seen in subsection 1.2.2. In function spaces, a property is generic if it holds on a dense open set. Let us clarify what we understand by generic property when considering a parametric family of dynamical systems. In such a setting, we can use the split function to define a topology in the function space $X = \{f_\gamma(x) : |\gamma - \gamma_0| < \gamma_1\}$ for a fixed value of the parameter γ_1 close to γ_0. Under the assumption of ρ being monotonic with respect to γ locally around γ_0, one can define the metric $d : X \times X \to \mathbb{R}$ defined as $d(f_\gamma, f_{\gamma'}) = |\rho(\gamma) - \rho(\gamma')|$, $\forall f_\gamma, f_{\gamma'} \in X$. The assumption that ρ is monotonic is essential so that d is a metric, because it implies that $d(f_\gamma, f_{\gamma'}) = 0$ if and only if $\gamma = \gamma'$. Therefore (X, d) is a metric space, which in particular is a topological space with the topology described by the open sets $U_\epsilon = \{f_\gamma(x) \in X : d(f_\gamma, f_{\gamma_0}) < \epsilon\}$. Then, Prop 1.16 means that the property of having a homoclinic orbit to a hyperbolic point is non-generic in the sense that there can not exist any open set U_ϵ dense in X such that f_γ has a homoclinic orbit $\forall f_\gamma \in U_\epsilon$.

Chapter 2

Dynamics of a Shilnikov System

In Chapter 1 we saw that some changes in the phase space are expected to occur in systems containing homoclinic orbits to hyperbolic equilibria. This chapter aims to study the main properties of the dynamics of a system presenting a Shilnikov bifurcation. Such bifurcation is related to a specific configuration of the phase space of a $3-$dimensional system having a homoclinic orbit to a fixed point. We will also study the richness of dynamics that take place in a neighbourhood of the homoclinic orbit. This study leads to the statement and proof of the Shilnikov theorem.

To do that, we will consider a parametric system $\dot{x} = f(x,\gamma) = f_\gamma(x)$, with $f : \mathbb{R}^n \times \mathbb{R} \to \mathbb{R}^n$ smooth, having a homoclinic orbit Γ_0 to a saddle-focus hyperbolic equilibrium that we assume to be at the origin for $\gamma = \gamma_0$. We will also assume that $Df_{\gamma_0}(0)$ has a real eigenvalue $\lambda > 0$ and two complex eigenvalues $\omega, \overline{\omega}$ such that $\omega = \alpha + i\beta$ with $\alpha < 0$. Therefore, as follows from the stable manifold theorem (see Theorem 1.14) the systems f_γ have an unstable $1-$dimensional invariant manifold and a $2-$dimensional invariant one in which the flow spirals towards the origin. As explained in section 1.2.3, we will also assume that $\rho'(\gamma_0) \neq 0$, where $\rho(\gamma)$ is the split function.

2.1 Reduction to a discrete system

The most important properties of a system in which a Shilnikov bifurcation occurs can be studied reducing the original continuous dynamical system into a discrete dynamical system. This is achieved by taking advantage of the recurrent properties of the dynamics near the homoclinic orbit to introduce a suitable Poincaré section and to reduce the system to a discrete one defined by the cor-

responding Poincaré map. In particular, to build this new discrete system, it is crucial to understand the dynamics in a neighbourhood of the saddle-focus of f_γ. We present a detailed study on the flow in this neighbourhood in subsection 2.1.1.

For the derivation of the Poincaré map, we closely follow the references [GH13] and [HSD12]. In particular, we analyze the Poincaré map to a section chosen as in such references. However, similar return maps using different sections can be found in the literature, as in [Wig13].

2.1.1 Local flow and linear dynamics

The Hartman-Grobman Theorem (see [Tes12]) establishes that the dynamics of the linear system associated to f_γ in the origin behaves similarly to the dynamics of f_γ in a neighbourhood of the equilibrium. Therefore, it is not needed to describe f_γ explicitly because the dynamics manifested in the Shilnikov bifurcation is determined by its linear part.

Theorem 2.1. (Hartman-Grobman) Consider $X : U \to \mathbb{R}^n$, where $U \subset \mathbb{R}^n$ is an open set, $X \in \mathcal{C}^1(U)$ and a hyperbolic equilibrium x_* of X. Let $Y : \mathbb{R}^n \to \mathbb{R}^n$ be the linear vector field defined by $Y(y) = DX(x_*) \cdot y$. Then X and Y are locally topologically conjugate, that is, there exist neighbourhoods U_*, V_* of x_* and $y_* = 0$ respectively and a homeomorphism $h : U_* \to V_*$ such that $h \circ \varphi = \psi \circ h$, where φ is the flux of X and ψ is the flux of Y.

All those premises set the following linear system $X' = AX$ underlying all the information on the flow of $f_\gamma(x)$ around the saddle-focus for an arbitrary γ in a neighbourhood of γ_0:

$$\begin{pmatrix} \dot{x} \\ \dot{y} \\ \dot{z} \end{pmatrix} = \begin{pmatrix} \alpha & -\beta & 0 \\ \beta & \alpha & 0 \\ 0 & 0 & \lambda \end{pmatrix} \begin{pmatrix} x \\ y \\ z \end{pmatrix},$$

where $\alpha = \alpha(\gamma), \beta = \beta(\gamma)$ and $\lambda = \lambda(\gamma)$ determine the eigenvalues of the saddle-focus points of f_γ. Its solution for an initial condition $X_0 = (x_0, y_0, z_0)$ is the flow $X(t) = X_0 exp(tA)$, which can be computed using analytic methods. First of all, tA can be split as the sum of two sparse matrices.

$$tA = tB + tC = \begin{pmatrix} t\alpha & 0 & 0 \\ 0 & t\alpha & 0 \\ 0 & 0 & t\lambda \end{pmatrix} + \begin{pmatrix} 0 & -t\beta & 0 \\ t\beta & 0 & 0 \\ 0 & 0 & 0 \end{pmatrix}$$

A property of the exponential of a matrix simplifies the computations.

$$tB \cdot tC = tC \cdot tB \implies e^{tA} = e^{tB} \cdot e^{tC}$$

Since tB is a diagonal matrix, its exponential can be obtained from the definition of the exponential of a matrix as a power series, see [Sot79],

$$e^{tB} = \sum_{n=0}^{\infty} \frac{(tB)^n}{n!} = \begin{pmatrix} \sum_{n=0}^{\infty} \frac{(t\alpha)^n}{n!} & 0 & 0 \\ 0 & \sum_{n=0}^{\infty} \frac{(t\alpha)^n}{n!} & 0 \\ 0 & 0 & \sum_{n=0}^{\infty} \frac{(t\lambda)^n}{n!} \end{pmatrix} = \begin{pmatrix} e^{t\alpha} & 0 & 0 \\ 0 & e^{t\alpha} & 0 \\ 0 & 0 & e^{t\lambda} \end{pmatrix}$$

The first powers of tC are the following:

$$(tC)^0 = Id, \quad tC = t\beta \begin{pmatrix} 0 & -1 & 0 \\ 1 & 0 & 0 \\ 0 & 0 & 0 \end{pmatrix}, \quad (tC)^2 = -(t\beta)^2 Id$$

$$(tC)^3 = -(t\beta)^3 \begin{pmatrix} 0 & -1 & 0 \\ 1 & 0 & 0 \\ 0 & 0 & 0 \end{pmatrix}, \quad (tC)^4 = (t\beta)^4 Id = (t\beta)^4 C^0$$

The powers of tC start getting repeated at that point, hence we know them all. Consequently, the exponential of tC is

$$\begin{aligned} e^{tC} = \sum_{n=0}^{\infty} \frac{(tC)^n}{n!} &= \begin{pmatrix} \sum_{n=0}^{\infty} (-1)^n \frac{(t\beta)^{2n}}{(2n)!} & -\sum_{n=0}^{\infty} (-1)^n \frac{(t\beta)^{2n+1}}{(2n+1)!} & 0 \\ \sum_{n=0}^{\infty} (-1)^n \frac{(t\beta)^{2n+1}}{(2n+1)!} & \sum_{n=0}^{\infty} (-1)^n \frac{(t\beta)^{2n}}{(2n)!} & 0 \\ 0 & 0 & 1 \end{pmatrix} = \\ &= \begin{pmatrix} \cos(t\beta) & -\sin(t\beta) & 0 \\ \sin(t\beta) & \cos(t\beta) & 0 \\ 0 & 0 & 1 \end{pmatrix} \end{aligned} \tag{2.1}$$

In conclusion, the flow of the linear system near the origin for an initial condition $X_0 \in \mathbb{R}^3$ is:

$$X(t) = X_0 e^{tA} = \begin{pmatrix} e^{t\alpha}(x_0 \cos(t\beta) - y_0 \sin(t\beta)) \\ e^{t\alpha}(x_0 \sin(t\beta) + y_0 \cos(t\beta)) \\ z_0 e^{t\lambda} \end{pmatrix} \tag{2.2}$$

From the expression (2.2) we see that the $2-$dimensional stable and the $1-$dimensional unstable manifolds of the origin are contained in the horizontal plane $z = 0$ and in the vertical line $x = y = 0$, respectively.

2.1.2 Construction of a Poincaré map

Without loss of generality, we will assume from now on that the saddle-focus of the systems f_γ for $\gamma \approx \gamma_0$ lays in the origin. This can be easily achieved by applying affine transformations over the phase space.

The current aim is to reduce f_γ to a discrete dynamical system defined by a Poincaré map using the properties of the linear flow of section 2.1.1. The main steps of the construction of this Poincaré map can be found in [SS07] and in [GH13] for $\gamma = \gamma_0$. Here, we will provide several details of this construction and justify that it can be carried for values of the parameter $\gamma \approx \gamma_0$.

Assume that the homoclinic orbit Γ_0 is given by the positive branch of the unstable manifold of the origin. Moreover, we assume that the other branch from the unstable manifold escapes to infinity (or does not return to the region of interest).

The local map describing the passage near the saddle-focus. To begin with, let us consider two transversal surfaces Σ_0 and Σ_1 in a neighbourhood of the origin. Concretely, we consider

$$\Sigma_0 = \{(x, y, z) \in \mathbb{R}^3 : x^2 + y^2 = r_0^2, 0 < z < z_1\}$$

and

$$\Sigma_1 = \{(x, y, z) \in \mathbb{R}^3 : x^2 + y^2 < r_0^2, z = z_1\},$$

where the constants $r_0 > 0$ and $z_1 > 0$ are considered small enough so that, by Theorem 2.1, the flow of $f_\gamma(x)$ is topologically conjugated to $X(t)$ defined in (2.2), in the closed solid cylinder C_+ delimited by Σ_0, Σ_1 and the stable plane $z = 0$.

Remark 2.2. We can choose C_+ uniformly in γ, because if we consider the systems $f_\gamma(x)$ for $\gamma \in (\gamma_0 - \epsilon, \gamma_0 + \epsilon)$ and $\epsilon > 0$, then the cylinder C_+ defined as the intersection of all cylinders in which the flow of $f_\gamma(x)$ is linear for $\gamma \in (\gamma_0 - \epsilon, \gamma_0 + \epsilon)$, satisfies the desired properties (transversality and conjugacy with linear dynamics) for all possible values of γ.

One can find in [HSD12] the computations from section 2.1.1 with fixed values for α, β and λ. However, the orbits from C_+ with those values do not show an illustrative phase portrait of the actual scenario. Consequently, we display in Figure 2.1 the shape of an orbit inside C_+ given by the linear flow (2.2) with values $\alpha = -0.5, \beta = -10, \lambda = 0.1$, that provide a visually more accurate representation of the actual dynamics in C_+.

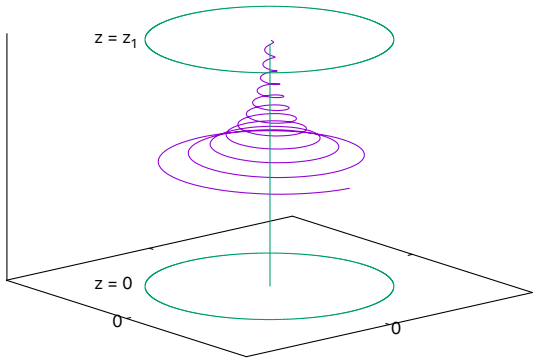

Figure 2.1: Positive orbit of a point from Σ_0 inside C_+.

Take a point $X_0 = (x_0, y_0, z_0) \in C_+$ and let us introduce cylindrical coordinates $x = r\cos(\theta), y = r\sin(\theta), z = z$. We will denote as C the change from Cartesian to cylindrical coordinates using those relations. Then, the evolution of the radial coordinate along the solution is, according to (2.2):

$$r = \sqrt{x^2 + y^2} = e^{t\alpha}\sqrt{x_0^2 + y_0^2} = e^{t\alpha} r_0$$

As time advances, r decreases and $z = z_0 e^{t\lambda}$ increases because $\alpha < 0 < \lambda$. Therefore, $\forall X_0 \in C_+ \setminus \{z = 0\}$, it is satisfied that the first crossing of $Or(X_0)$ with Σ_1 gives a point $P_0 \in \mathbb{R}^3$. In particular, we can define a map $\psi_1 : \Sigma_0 \to \Sigma_1$ such that $\forall X_0 \in \Sigma_0$, its image by ψ_1 is given by the first crossing of its orbit with Σ_1.

The image of ψ_1 can be described explicitly by determining the time of flight of a point through its orbit from Σ_0 to Σ_1. One has:

$$z_1 = e^{t\lambda} z_0 \iff t = \frac{1}{\lambda}\log\left(\frac{z_1}{z_0}\right)$$

The image of ψ_1 is obtained by substituting the flight time into the flow $X(t)$. Setting

$$\kappa(z) = \frac{\beta}{\lambda}\log\left(\frac{z_1}{z}\right) \tag{2.3}$$

to simplify notation, one obtains

$$\psi_1\begin{pmatrix} x \\ y \\ z \end{pmatrix} = \begin{pmatrix} \left(\frac{z_1}{z}\right)^{\frac{\alpha}{\lambda}} \left(x\cos(\kappa(z)) - y\sin(\kappa(z))\right) \\ \left(\frac{z_1}{z}\right)^{\frac{\alpha}{\lambda}} \left(x\sin(\kappa(z)) + y\cos(\kappa(z))\right) \\ z_1 \end{pmatrix} \tag{2.4}$$

The global map. Let W^u be the unstable invariant manifold of the saddle-focus of $f_\gamma(x)$, and define $Q = W^u \cap \Sigma_1 = (0, 0, z_1)$. By continuity with respect to initial

conditions, since the flight time from Σ_1 to Σ_0 is finite for all points in Σ_1, there exist a global diffeomorphism ψ_2 that maps any $p \in \Sigma_1$ in a neighbourhood of Q to $\psi_2(p)$ which is the first intersection of $Or(p)$ with $\overline{\Sigma_0}$, where:

$$\overline{\Sigma_0} = \{(x, y, z) \in \mathbb{R}^3 : x^2 + y^2 = r_0^2, |z| < z_2\}$$

for a certain value $z_2 < z_1$. Note that this section extends to negative values of z to capture all orbits of the global map. From now on, applying a rotation to the coordinates around the z-axis, we will assume that $\psi_2(Q) = (r_0, 0, z)$ for an appropriate $0 < z < z_2$. This deduces to fix a proper origin of the angle of the cylindrical coordinates. In particular, if $\gamma = \gamma_0$ then $\psi_2(Q) = (r_0, 0, 0)$.

The return map to Σ_0. Now we want to define the domain of a Poincaré map described by $\psi_2 \circ \psi_1$. Notice that points $p \in \overline{\Sigma_0} \backslash \Sigma_0$ are situated below W^s, the stable invariant manifold of the saddle-focus. Then $Or(p)$ will never cross Σ_1 again because we are assuming that the lower branch of the unstable manifold escapes from the region of interest.

In order to define a Poincaré map, we need to introduce a suitable region in Σ_0 where the return is well defined. Consider $\gamma = \gamma_0$ and a small region nearby $\psi_2(Q) = (r_0, 0, 0)$ defined as

$$\mathcal{S} = \{(r, \theta, z) : r = r_0, |\theta| < \delta, 0 < z < \epsilon\} \subset \Sigma_0 \tag{2.5}$$

where ϵ is small enough for $\psi_1(\mathcal{S})$ to be contained in the domain of ψ_2, and the exact conditions on the small value $\delta > 0$ will be stated in subsection 2.1.3. Notice that $\mathcal{S}$ is defined taking as reference the system $f_{\gamma_0}(x)$, but the same region is valid $\forall \gamma \approx \gamma_0$ as long as $\psi_2(Q) \in \mathcal{S}$ because transversality is a generic property. With this domain $\mathcal{S}$, one can see the function $(\psi_2 \circ \psi_1)$ as a diffeomorphism that maps points from $\mathcal{S}$ to points on $\mathcal{S}$. The corresponding Poincaré return map $\mathcal{P}$ to $\mathcal{S}$ defines a $2-$dimensional smooth discrete system. Let Π the projection onto the (θ, z) variables and note that Π restricted to Σ_0 defines a diffeomorphism. Then, the image of the Poincaré map is $\mathcal{P}(\theta, z) = \Pi \circ C \circ \psi_2 \circ \psi_1 \circ C^{-1} \circ \Pi^{-1}(\theta, z)$.

2.1.3 Iteration of the Poincaré map

The current objective is to determine the image of $\mathcal{S}$ by $\mathcal{P}$. If we set θ to a constant value $\theta_0 \in [0, 2\pi)$, points $(\psi_1 \circ C^{-1})(r_0, \theta_0, z)$ for $z \in (0, z_1)$ form a spiral in Σ_1 with centre Q. To see this, we note that denoting by $\tilde{\psi}_1$ the restriction of ψ_1 to the vertical line $\{y = \tan(\theta_0)x\} \cap \Sigma_0$, one has:

$$\tilde{\psi}_1(z) = \left(r_0 \left(\tfrac{z_1}{z}\right)^{\frac{\alpha}{\lambda}} \cos(\theta_0 + \kappa(z)), r_0 \left(\tfrac{z_1}{z}\right)^{\frac{\alpha}{\lambda}} \sin(\theta_0 + \kappa(z)), z_1\right)^T$$

The spiral structure is easily seen since, identifying the plane $z = z_1$ with the complex plane with complex coordinate $w = x + iy$, the two first components of $\tilde{\psi}_1(z)$ define a point such that

$$\begin{aligned} w = w(z) &= r_0 \left(\frac{z_1}{z}\right)^{\frac{\alpha}{\lambda}} \left(\cos\left(\theta_0 + \kappa(z)\right) + i \sin\left(\theta_0 + \kappa(z)\right)\right) = \\ &= r_0 \left(\frac{z_1}{z}\right)^{\frac{\alpha}{\lambda}} e^{i(\theta_0 + \kappa(z))} \end{aligned} \tag{2.6}$$

Since $z < z_1$ and $\alpha < 0 < \lambda$, the modulus $r_0(\frac{z_1}{z})^{\frac{\alpha}{\lambda}}$ is increasing and the argument goes through $[0, 2\pi)$ periodically because $\kappa(z) = \frac{\beta}{\lambda} \log(\frac{z_1}{z})$ is a monotonic function. Those properties define a logarithmic spiral with radius $r_0(\frac{z_1}{z})^{\frac{\alpha}{\lambda}}$ in Σ_1 that spirals infinitely many times around Q as z tends to 0. Figure 2.2 shows one of these spirals for a certain fixed value of θ.

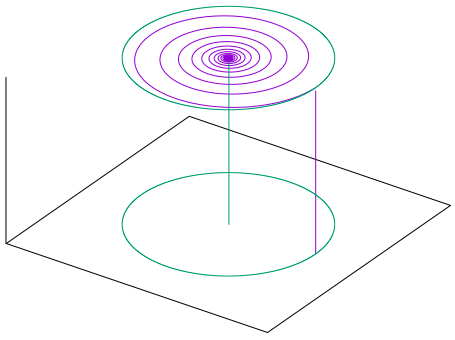

Figure 2.2: Vertical line in Σ_0 and its image by ψ_1 in Σ_1.

Let $\varphi(t, x)$ be the flow of $f_\gamma(x)$ outside C_+ and let t_* be the flight time from $Q = (0, 0, z_1) \in \Sigma_1$ to $\psi_2(Q) \in \overline{\Sigma_0}$ throughout φ. Then, for any fixed argument $\theta = \theta_0$, the spiral $\{\tilde{\psi}_1(z) : z \in (0, z_1)\} \subset \Sigma_1$ is mapped diffeomorphically by φ into $S_{t_*} = \{\varphi(t_*, \tilde{\psi}_1(z)) : z \in (0, z_1)\}$. The Tubular Flux Theorem guarantees that there exist an open neighbourhood V of $\psi_2(Q)$ such that $f_{\gamma|_V}$ and the vector field $Y(y) = \overrightarrow{e_1}$ are C^1-conjugated. Consequently, φ maps points from S_{t_*} diffeomorphically into $\overline{\Sigma_0}$, thus ψ_2 maps spirals from Σ_1 diffeomorphically into $\overline{\Sigma_0}$. In particular, vertical lines in $\mathcal{S}$ are mapped by $\psi_2 \circ \psi_1$ into spirals with centre $\psi_2(Q)$ inside $\overline{\Sigma_0}$, and the same happens with $\mathcal{P}$ because C and Π are smooth and one-to-one. Notice that the value of ϵ from the definition of $\mathcal{S}$ can be taken sufficiently small so that $\mathcal{S} \subseteq V$.

We know that up to this point, there is freedom choosing the parameter δ that defines the section $\mathcal{S}$, see (2.5). We can then choose δ large enough compared to ϵ so that for each vertical segment $I \subset \mathcal{S}$, the intersection of $\mathcal{S}$ with the diffeomorphic spiral $(\psi_2 \circ \psi_1)(I)$ is the union of vertical curves that do not cross the vertical boundaries of $\mathcal{S}$ transversally. Figure 2.3 illustrates the intersection of $\psi_2 \circ \psi_1(\mathcal{S})$ with $\mathcal{S}$ choosing the value of δ as specified.

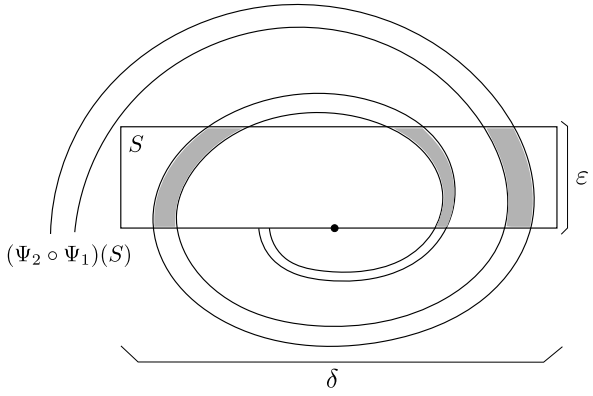

Figure 2.3: First iteration of $\mathcal{S}$ by $\psi_2 \circ \psi_1$ and its intersection with $\mathcal{S}$.

Next, we determine a subinterval $(z', z'') \subset (0, z_1)$ on the vertical line $\{\theta = \theta_0\} \cap \Sigma_0$ such that the diffeomorphic spiral $\{\mathcal{P}(\theta_0, z) : z \in (z', z'')\}$ makes approximately one turn around $\psi_2(Q) = W^u \cap \Sigma_0$. These intervals will be important later: we will see that a suitable construction based on a covering of the vertical line $\{\theta = \theta_0\} \cap \Sigma_0$ leads to the existence of infinitely many horseshoes, see sections 3 and 4.

Fixed $\theta = \theta_0$ and $z \in (z', z'')$ where $0 < z' < z'' < \epsilon$, the logarithmic spiral $\{\tilde{\psi}_1(z) : z \in (z', z'')\}$ makes exactly one full turn when $\kappa(z') - \kappa(z'') = 2\pi$, see (2.3).

$$\kappa(z') - \kappa(z'') = 2\pi \iff \frac{\beta}{\lambda}\left(\log\left(\frac{z_1}{z'}\right) - \log\left(\frac{z_1}{z''}\right)\right) = 2\pi \iff$$
$$\iff \log\left(\frac{z''}{z'}\right) = \frac{2\pi\lambda}{\beta} \iff \frac{z''}{z'} = e^{\frac{2\pi\lambda}{\beta}}$$

Since ψ_2 is a diffeomorphism, the image of this spiral by ψ_2 will make approximately one full turn too in $\overline{\Sigma_0}$.

Furthermore, from (2.6) one has that the distance from Q to $\tilde{\psi}_1(z)$ for $z \in (z', z'')$ is $r_0 \left(\frac{z_1}{z}\right)^{\frac{\alpha}{\lambda}}$. Therefore, the ratio $\left(\frac{z_1}{z}\right)^{\frac{\alpha}{\lambda}} / z$ as z tends to 0 determines if $\tilde{\psi}_1(z)$ is

further or closer to Q than z to 0. Namely, it gives information about whether $\mathcal{P}$ is expansive or a contraction mapping. Figure 2.4 illustrates the distances involved in that ratio. It is convenient to express that limit in the following way:

$$\lim_{z\to 0} \frac{\left(\frac{z_1}{z}\right)^{\frac{\alpha}{\lambda}}}{z} = z_1^{\frac{\alpha}{\lambda}} \lim_{z\to 0} \frac{1}{z^{\frac{\alpha}{\lambda}+1}} \tag{2.7}$$

Before interpreting the value of this limit, let us introduce notation on some values that will be used repeatedly in the forthcoming sections.

Definition 2.3. A saddle value σ of a saddle-focus is the sum of the positive eigenvalue and the negative real part of the complex eigenvalue.

The value of the limit (2.7) varies depending on $\sigma = \alpha + \lambda$. It will be assumed that $\alpha \neq -\lambda$ excluding the case $\sigma = 0$ which was first studied by L. Belyakov in [Bel84]. Therefore, we will only distinguish the cases $\sigma > 0$ and $\sigma < 0$. One has:

$$\sigma > 0 \implies \alpha + \lambda > 0 \implies \frac{\alpha}{\lambda} + 1 > 0 \implies \lim_{z\to 0} \frac{1}{z^{\frac{\alpha}{\lambda}+1}} = \infty$$

$$\sigma < 0 \implies \alpha + \lambda < 0 \implies \frac{\alpha}{\lambda} + 1 < 0 \implies \lim_{z\to 0} \frac{1}{z^{\frac{\alpha}{\lambda}+1}} = 0$$

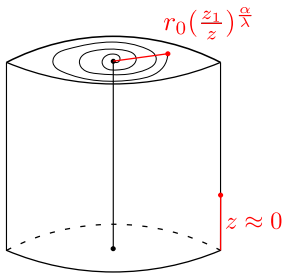

$$\sigma > 0 \implies r_0\left(\tfrac{z_1}{z}\right)^{\frac{\alpha}{\lambda}} > z$$
$$\sigma < 0 \implies r_0\left(\tfrac{z_1}{z}\right)^{\frac{\alpha}{\lambda}} < z$$

Figure 2.4: Values involved in the limit of the ratio and their relation.

Let us show that the Poincaré map $\mathcal{P}$ contracts areas if $\sigma < 0$ and expands areas if $\sigma > 0$. To see that, we consider $\psi_1^C = C \circ \psi_1 \circ C^{-1}$ and $\psi_2^C = C \circ \psi_2 \circ C^{-1}$, that is, the maps ψ_1 and ψ_2 expressed in cylindrical coordinates. We shall check that the area contraction/expansion properties (depending on the sign of σ) of $\mathcal{P}$ become arbitrary large for small enough values of z. First, note that $D(\Pi^{-1} \circ \psi_2^C \circ \Pi)$ is bounded since the flight time from Σ_1 to Σ_0 is also bounded. This means that the area expansion/contraction properties of $\mathcal{P}$ can be read from ψ_1. In other words, one can consider that

$$\psi_2^C(r, \theta, z) = (r_0, \theta, r_0(\frac{z_1}{z})^{\frac{\alpha}{\lambda}}),$$

because the ignored effects are bounded. Then, the return map can be defined as $P(\theta, z) = (\theta + \kappa(z), r_0(\frac{z_1}{z})^{\frac{\alpha}{\lambda}})$. With that expression, one can check that

$$|Det(D\mathcal{P}(\theta, z))| = -\frac{\alpha r_0 z_1^{\frac{\alpha}{\lambda}}}{\lambda z^{\frac{\alpha}{\lambda}+1}}$$

As we saw in (2.7), the limit of that value when z tends to 0 is $+\infty$ if $\sigma > 0$ and 0 if $\sigma < 0$, which means that when z tends to 0, the Poincaré map $\mathcal{P}$ is expansive if $\sigma > 0$ and it is a contraction mapping if $\sigma < 0$. The bifurcations taking place whenever $\sigma > 0$ and $\sigma < 0$ lead to a different type of phenomena. In section 2.2 we will study the case $\sigma < 0$ completely, but the case $\sigma > 0$, which exhibits richer dynamics, is postponed to Chapter 4 because it requires a technical overview of the horseshoe map covered in Chapter 3.

2.2 Case $\sigma < 0$

To study the dynamics of $\mathcal{P}$ when $\sigma < 0$, we will make the additional assumption that $\rho(\gamma) > 0$ is sufficiently close to 0, where ρ is the split function. Therefore, the unstable manifold of the saddle-focus will stay above the stable manifold in a neighbourhood of the origin. Consequently, any iteration of $\mathcal{P}$ lays in Σ_0, which means that all iterations are well-defined. The case $\rho(\gamma) < 0$ when $\sigma < 0$ does not present any new dynamical phenomena in the region of interest.

In section 2.1.3 we saw that for $\sigma < 0$, the Poincaré map $\mathcal{P}$ is a contraction mapping defined on the domain $\mathcal{S}$. Under those hypotheses, the Banach Fixed Point Theorem states a significant consequence on the dynamics of $\mathcal{P}$.

Theorem 2.4. (Banach Fixed Point Theorem) Let X be a complete metric space and consider a continuous contraction mapping $f : X \to X$, i.e., there exists a constant $k \in (0, 1)$ such that

$$d(f(x), f(y)) \leq k\, d(x, y), \text{for all } x, y \in X$$

Then, f has a unique fixed point p and $\forall x_0 \in X$, $x_{n+1} = f(x_n)$ converges to p.

Proof. See section A.2 in Appendix A. □

Consequently, by Theorem 2.4, $\mathcal{P}$ has a unique attracting fixed point $p \in \mathcal{S}$. Recalling that $\mathcal{P}$ is a Poincaré map, the stable fixed point p corresponds to a stable limit cycle in our original system f_γ. In conclusion, if $\sigma < 0$, systems f_γ sufficiently

$\mathcal{C}^1 - close$ to f_{γ_0} with $\rho(\gamma) > 0$ have a unique stable limit cycle in a neighbourhood of the homoclinic orbit Γ_0 of the system f_{γ_0}. In particular, this stable limit cycle is the $\omega - limit$ of points that lay in a tubular neighbourhood of the unstable manifold of x_0. Figure 2.5 illustrates a representative scenario with that limit cycle.

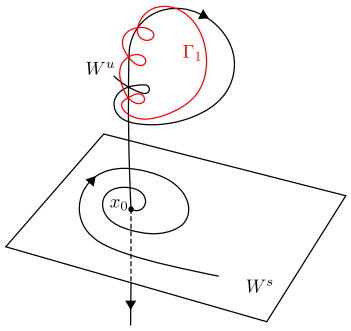

Figure 2.5: Stable limit cycle Γ_1 when $\sigma < 0$.

Remark 2.5. This result is valid for $\rho(\gamma) > 0$ sufficiently small. As it was justified in subsection 2.1.2, the Poincaré map $\mathcal{P}$ can be defined for small values of $\rho(\gamma) \geq 0$. Notice that when $\rho(\gamma)$ tends to 0, the stable limit cycle accumulates onto the homoclinic orbit, which does not intersect $\mathcal{S}$. Thus, there is not an appearance of such a limit set until $\rho(\gamma)$ becomes strictly positive. One says that the limit cycle is born for $\rho(\gamma) > 0$ from the homoclinic connection.

Additionally, one can see that the Shilnikov bifurcation for $\sigma < 0$ resembles the $2-$dimensional homoclinic bifurcation, which is completely described by the Andronov-Leontovich Theorem (see [Kuz13]) and visualized in Figure 2.6. The existence of such a limit cycle for $2-$dimensional flows follows indeed from the Poincaré-Bendixson theorem, see [Sot79].

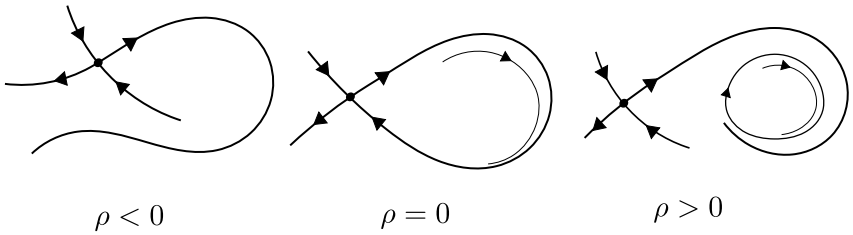

Figure 2.6: Here we illustrate the planar homoclinic bifurcation. The appearance of a stable limit cycle resembles the Shilnikov bifurcation with $\sigma < 0$.

Chapter 3

The Horseshoe Map

With the notation from section 2.1.3, when $\sigma > 0$, the iterations of $\mathcal{S}$ by $\mathcal{P}$ resemble the horseshoe map, a two-dimensional discrete dynamical system presenting chaotic behaviour. The horseshoe map is noteworthy because its complicated dynamics can be studied in depth using symbolic dynamics, and many systems have the horseshoe map as a subsystem.

In this section, we will describe the horseshoe map, show its most interesting properties in terms of dynamics, and generalize it along with the introduction of the shift map to determine a series of conditions under which a two-dimensional dynamical system is topologically conjugated to the horseshoe map. All of that will be useful to understand the dynamics of the parametric system f_γ when $\sigma > 0$.

3.1 Construction and properties of the horseshoe map

In this section, we construct the horseshoe map and study some of its properties, which show the rich dynamics that this discrete system has. The main ideas and definitions in this section are from [GH13], [HSD12], [Mos01] and [Kuz13].

The horseshoe map is a homeomorphism $f : \mathbb{R}^2 \to \mathbb{R}^2$ defined by the following procedure which is illustrated in Figure 3.1:

1. Take a compact square $\mathcal{S} \subset \mathbb{R}^2$.
2. Contract its width and expand its height.
3. Fold it from the middle giving the resulting set a horseshoe like shape.
4. Place it over the original square $\mathcal{S}$ so that the intersection $f(\mathcal{S}) \cap \mathcal{S}$ is the union of two vertical strips.

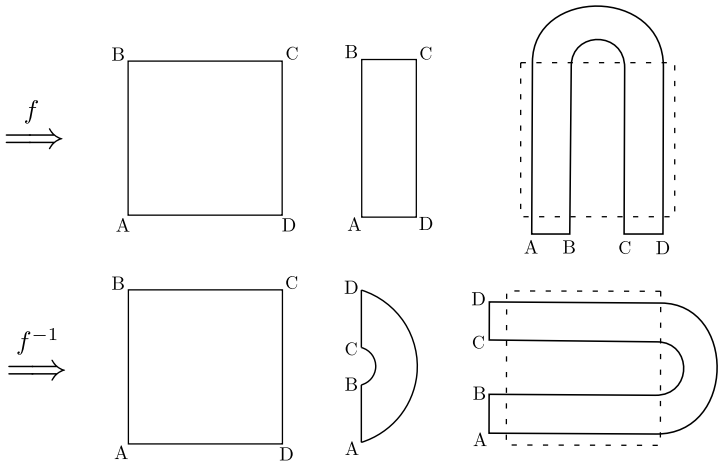

Figure 3.1: Horseshoe map and its inverse step by step.

The inverse map of f folds horizontally mapping the original square $\mathcal{S}$ to two horizontal strips. The exact shape of $f(\mathcal{S})$ or $f^{-1}(\mathcal{S})$ is not relevant, hence we can assume that the expansions and contractions of $\mathcal{S}$ are linear by factors λ, μ respectively with $\lambda > 2$ an $0 < \mu < \frac{1}{2}$. That assumption keeps the map well defined, and it forces the two strips $f(\mathcal{S}) \cap \mathcal{S}$ to be two vertical rectangles V_0, V_1 and the two strips $f^{-1}(\mathcal{S}) \cap \mathcal{S}$ to be two horizontal rectangles H_0, H_1.
If we iterate f one more time, the two vertical rectangles V_0 and V_1 are transformed into four thinner vertical rectangles $V_{0,0}, V_{01}, V_{10}, V_{11}$ such that $V_{00} \cup V_{01} \subset V_0$ and $V_{10} \cup V_{11} \subset V_1$. We can rewrite this as:

$$\mathcal{S} \cap f(\mathcal{S}) \cap f^2(\mathcal{S}) = V_{00} \cup V_{01} \cup V_{10} \cup V_{11}$$

The same happens for the inverse map:

$$\mathcal{S} \cap f^{-1}(\mathcal{S}) \cap f^{-2}(\mathcal{S}) = H_{00} \cup H_{01} \cup H_{10} \cup H_{11}$$

In general $\mathcal{S} \cap f^k(\mathcal{S})$ is the union of 2^k vertical rectangles and $\mathcal{S} \cap f^{-k}(\mathcal{S})$ is the union of 2^k horizontal rectangles for every $k \in \mathbb{N}$. That property is shown for $k = 2$ in Figure 3.2. Moreover, notice that by how f is constructed, the following equalities are satisfied for every $k \in \mathbb{Z}$:

$$f^k(f^{-k}(\mathcal{S}) \cap S) = f^k(\mathcal{S}) \cap \mathcal{S} \tag{3.1}$$

In other words, horizontal rectangles of height λ^{-k} are mapped by f^k to vertical rectangles of width μ^k and vertical rectangles of width μ^k are mapped by f^{-k} to horizontal rectangles of height λ^{-k} for every $k \in \mathbb{N}$. The process justifying the

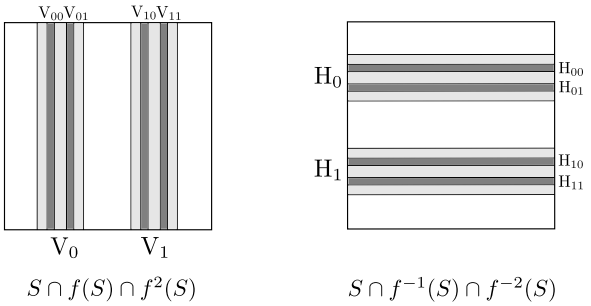

Figure 3.2: $\mathcal{S}$ intersected with the first two iterations of f.

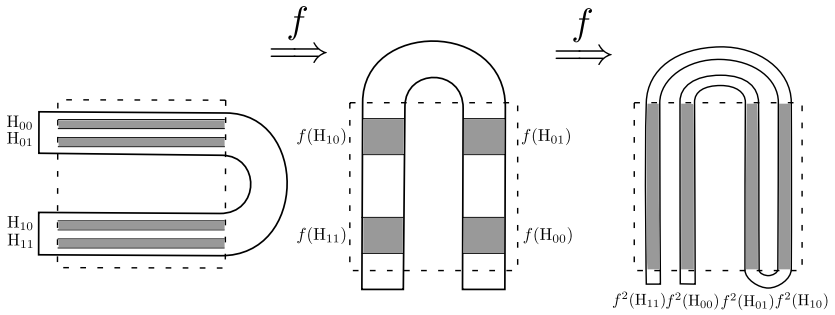

Figure 3.3: In this picture, we illustrate that $f^2(f^{-2}(\mathcal{S}) \cap \mathcal{S}) = f^2(\mathcal{S}) \cap \mathcal{S}$.

veracity of equation 3.1 when $k = 2$ is illustrated in Figure 3.3.

We are interested in the set of points invariant by $f^k, \forall k \in \mathbb{Z}$. This set is important because every iteration of f is well defined over it, but it has other properties that we will show in the following results and sections. This invariant set Λ can be defined using different expressions:

$$\Lambda = \{x \in \mathcal{S} : f^k(x) \in \mathcal{S}, \forall z \in \mathbb{Z}\} = \bigcap_{k \in \mathbb{Z}} f^k(\mathcal{S})$$

Symbolic dynamics facilitate the study of the dynamics of the horseshoe map. The following lemma establishes the relation between the invariant set Λ and the set of bi-infinite sequences of two symbols. A guideline of the proof can be found in [Kuz13]. In this work, we rewrite it giving all the details.

Lemma 3.1. There is a one-to-one correspondence $h : \Lambda \to \mathcal{A}_2^{\mathbb{Z}}$, where $\mathcal{A}_2^{\mathbb{Z}} = \{s = ...s_{-1} \cdot s_0 s_1 s_2..., \text{such that } s_i \in \{0, 1\}\}$. The sequence $b = h(f(x)) \in \mathcal{A}_2^{\mathbb{Z}}$ is obtained from the sequence $a = h(x) \in \mathcal{A}_2^{\mathbb{Z}}$ using the relation $b_k = a_{k+1}$. Additionally $\mathcal{A}_2^{\mathbb{Z}}$

has a metric defined by

$$d(a,b) = \sum_{k=-\infty}^{+\infty} \delta_k \cdot 2^{-|k|}, \quad \delta_i = \begin{cases} 0, \text{if } a_i = b_i \\ 1, \text{if } a_i \neq b_i \end{cases}$$

and h is a homeomorphism with that metric.

Proof. For any $x \in \Lambda$, we can construct the sequence $s = ...s_{-1} \cdot s_0 s_1 s_2...$ where:

$$s_k = \begin{cases} 0, & \text{if } f^k(x) \in H_0 \\ 1, & \text{if } f^k(x) \in H_1 \end{cases}$$

The sequence is well defined because $\Lambda \subset f^{-1}(\mathcal{S}) \cap \mathcal{S} = H_0 \cup H_1$ and by the definition of being invariant, $f^k(x) \in \mathcal{S}, \forall x \in \Lambda$ and $\forall k \in \mathbb{Z}$. Therefore, we can define $h : \Lambda \to \mathcal{A}_2^{\mathbb{Z}}$ mapping points $x \in \Lambda$ to their corresponding sequence of symbols.

The relation between h and f is given by the shift map $\sigma : \mathcal{A}_2^{\mathbb{Z}} \to \mathcal{A}_2^{\mathbb{Z}}$ defined as: $\sigma(a) = b$ if and only if $b_k = a_{k+1}, \forall k \in \mathbb{Z}$. It is satisfied that $h(f(x)) = \sigma(h(x))$ because $f^{k+1}(x) = f(f^k(x))$.

To prove that h is one-to-one, for any $m > 0$ define

$$R_m(s) = \{x \in \mathcal{S} : f^k(x) \in H_{s_k}, -m \leq k \leq m-1\}$$

which is the set of points with a fixed string of symbols in the centre of the sequence. If $-m \leq k \leq -1$, we have that $f^k(x) \in H_{s_k} \iff x \in f^{-k}(H_{s_k})$ which is the union of vertical rectangles of width μ^k because of (3.1). If $0 \leq k \leq m-1, f^k(x) \in H_{s_k} \iff x \in f^{-k}(H_{s_k})$, which is the union of horizontal rectangles of height $\lambda^{-(k+1)}$ because of the construction of f^{-1}. Therefore, $x \in R_m(s)$ if and only if x lays inside a rectangle of width μ^m and height λ^{-m}. Since $m > 0, 0 < \mu < \frac{1}{2}$ and $\lambda > 2$, the length of the diagonal of those rectangles tend to 0 as m tends to $+\infty$. This limit can be taken $\forall x \in \Lambda$ because $\Lambda \subset H_0 \cup H_1$ is invariant. Consequently, h is one-to-one because $\forall x, y \in \Lambda, h(x) = h(y) \implies x = y$.

Given $m \in \mathbb{N}$ and a point $x \in \Lambda$ such that $h(x) = s$, then for any point $y \in R_m(s)$ with $h(y) = t$, it is satisfied that $s_k = t_k$ for $-m \leq k \leq m-1$ because of the definition of $R_m(s)$. Using the distance between sequences given in the lemma:

$$d(s,t) = \sum_{k=-\infty}^{+\infty} \delta_k 2^{-|k|} = \sum_{k=-\infty}^{-m-1} \delta_k 2^{-|k|} + \sum_{k=m}^{+\infty} \delta_k 2^{-|k|} < 2^{2-m}$$

The function h is continuous because $\forall \epsilon > 0, \exists m > 0$ large enough with $2^{2-m} < \epsilon$ and $\exists \delta = \sqrt{\mu^{2m} + \lambda^{-2m}}$ such that $d_E(x,y) < \delta \implies d(h(x), h(y)) < 2^{2-m} < \epsilon$,

where d_E denotes the Euclidean distance. The continuity of h^{-1} is due to h being continuous, one-to-one and Λ compact.

Let us define $R(s_{-m},...,s_n) = \{x \in \mathcal{S} : f^k(x) \in H_{s_k}, -m, \leq k \leq n\}$. If we prove that $R(s_{-m},...,s_n) \neq \emptyset, \forall m,n \in \mathbb{N}$, then $\forall s \in \mathcal{A}_2^{\mathbb{Z}}, \exists x \in \mathcal{S}$ such that $h(x) = s$, which is the definition of h being onto. We saw in the proof that h is one-to-one that $R(s_0,...,s_n)$ is a horizontal rectangle of height $\lambda^{-(n+1)}$ and $R(s_{-m},...,s_{-1})$ is a vertical rectangle of width μ^{-m}. By definition:

$$R(s_{-m},...,s_n) = R(s_{-m},...,s_{-1}) \cap R(s_0,...,s_n)$$

That intersection is not empty because any vertical rectangle in $\mathcal{S}$ having the same height as $\mathcal{S}$ intersects any horizontal rectangle in $\mathcal{S}$ having the same width as $\mathcal{S}$. □

Remark 3.2. We proved that the dynamical systems $(\mathbb{Z}, \Lambda, f)$ and $(\mathbb{Z}, \mathcal{A}_2^{\mathbb{Z}}, \sigma)$ are topologically conjugated because $f(x) = h^{-1}(\sigma(h(x))), \forall x \in \Lambda$. In particular, h maps orbits of f in Λ to orbits of σ in $\mathcal{A}_2^{\mathbb{Z}}$.

Studying the chaotic behaviour of f solely from its construction is a difficult task. Symbolic dynamics is a powerful tool to show properties related to the periodicity of a discrete map, leading in some cases to chaotic behaviour. The following result uses the shift map presented in lemma 3.1 to show that the horseshoe map presents chaos in the form of dense sets of orbits of arbitrarily long periods.

Theorem 3.3. (Smale 1963) The horseshoe map f has a closed invariant set Λ containing a countable set of periodic orbits of arbitrarily long period, an uncountable set of non-periodic orbits and dense orbits.

Proof. A periodic orbit of period $k \geq 1$ for σ is a set of the form

$$\{\sigma^i(s) : 0 \leq i \leq k-1 \text{ and } s_j = s_{j+k}, \forall j \in \mathbb{Z}\}$$

Given $k \geq 1$, there are 2^k different sequences of k symbols $s'_0,...,s'_{k-1}$ with $s'_i \in \{0,1\}, \forall i \in \{0,...,k-1\}$. Then, for any of those 2^k finite sequences $s'_0,...,s'_{k-1}$, we can construct a sequence $s \in \mathcal{A}_2^{\mathbb{Z}}$ defined as:

$$s_i = s'_i \;\; \forall i \in \{0,...,k-1\} \text{ and } s_{i+k\cdot n} = s_i \;\; \forall i \in \{0,...,k-1\}, \forall n \in \mathbb{Z}$$

For any of those 2^k sequences, say s, the set $\{\sigma^i(s) : 0 \leq i \leq k-1\}$ is a periodic orbit of period k. It is clear that there are no more periodic orbits of period k because we considered all the possible variations of symbols. In consequence, the

amount of periodic orbits of σ of an arbitrary long period is countable. Since f and σ are topologically conjugate, the same happens for f.

Any point $x \in [0,1] \subset \mathbb{R}$ has a unique binary representation $0.s_1s_2s_3...$ with $s_i \in \{0,1\}, \forall i \in \mathbb{N}$. Therefore, for any point $(x,y) \in [0,1] \times [0,1] \subset \mathbb{R}^2$ we can take the binary representations of x and y and join them. Specifically, if $x = 0.s_1s_2s_3...$ and $y = 0.s_{-1}s_{-2}s_{-3}...$, we can create a sequence $s = ...s_{-3}s_{-2}s_{-1} \cdot s_1s_2s_3... \in \mathcal{A}_2^{\mathbb{Z}}$. Considering the orbits of those sequences by σ for all $(x,y) \in [0,1] \times [0,1]$, we get an uncountable amount of non-periodic orbits.

Take a sequence $s \in \mathcal{A}_2^{\mathbb{Z}}$ containing all finite sequences using the symbols 0 and 1.

$$s = ...0\ 1\ 00\ 10\ 01\ 11\ 000\ 100\ 010\ 001\ 110...$$

The distance between sequences given in Lemma 3.1 is small for sequences with similar symbols in the centre. Therefore, given a sequence $s' \in \mathcal{A}_2^{\mathbb{Z}}$, we can shift s as much as needed so that the arbitrarily long centre of s and s' coincide, decreasing the distance between s and s' as much as wanted. In other words, there are orbits in Λ passing arbitrarily close to any point in Λ, which means that f has dense orbits. □

The invariant set Λ and the shift map σ can be studied from the measure theoretical point of view. If $a \in \{0,1\}$, then we can define a measure $m(a) = p_a \in [0,1]$ satisfying $p_0 + p_1 = 1$. With that definition, $\{\mathcal{A}_2^{\mathbb{Z}}, \Sigma, m\}$ is a measure space, where Σ is the Borel algebra generated by the sets

$$B_{k_1,...,k_r}(a_1,...,a_r) = \{s \in \mathcal{A}_2^{\mathbb{Z}} : s_{k_1} = a_1, ..., s_{k_r} = a_r\} \text{ with } a_1,...,a_r \in \{0,1\}$$

For further details on this measure theoretical point of view, see [Mos01].

Proposition 3.4. The invariant set Λ is a null set, that is, $m(\Lambda) = 0$.

Proof. Using the notation from the proof of lemma 3.1 and the recently defined measure m, we deduce that $\forall n \in \mathbb{N}, \exists k \in \mathbb{N}$ such that $0 \leq k \leq 2n+1$ and $m(R(s_{-n},...,s_n)) = p_0^k \cdot p_1^{2n+1-k}$. Therefore, recalling that $p_0, p_1 \in [0,1]$ we have:

$$\lim_{n\to\infty} m(R(s_{-n},...,s_n)) = 0$$

We saw that points in Λ were actually rectangles of the form $R(s)$ with $s \in \mathcal{A}_2^{\mathbb{Z}}$. Consequently, $m(\Lambda)$ is the sum of the measures of null rectangles, that is, a sum of zeroes, which means that $m(\Lambda) = 0$ as we wanted to prove. □

3.2 Hyperbolicity and topological conjugacy with the horseshoe map

The horseshoe map with linear transformations explained in section 3.1 can be seen in hardly any system. Nonetheless, similar constructions arise in many dynamical systems and it would be interesting to establish a criterion determining if these systems do owe the properties of the horseshoe map and its invariant set. This generalisation of the horseshoe map is studied in [GH13], but most of the proofs of the involved results are outlined in [Mos01]. To begin with, we need to introduce the hyperbolic property of a set.

Definition 3.5. Let Λ be an invariant set of a discrete dynamical system $f : \mathbb{R}^n \to \mathbb{R}^n$. It is said that Λ is hyperbolic if $T_\Lambda \mathbb{R}^n = E^u_\Lambda \oplus E^s_\Lambda$ and there exist constants $C > 0, 0 < \lambda < 1$ such that:

1. $v \in E^u_x \implies |Df^{-n}(x) \cdot v| \leq C\lambda^n |v|$
2. $v \in E^s_x \implies |Df^{n}(x) \cdot v| \leq C\lambda^n |v|$

Remark 3.6. A full understanding of definition 3.5 requires further explanation:

- If M is a smooth manifold, then $T_\Lambda M$ is the set of tangent vectors to M at all points of Λ. The fact that $T_\Lambda \mathbb{R}^n = E^u_\Lambda \oplus E^s_\Lambda$ implies that for each $x \in \Lambda$, $T_x\mathbb{R}^n$ is the direct sum of the vector spaces E^u_x and E^s_x.
- $Df : T_\Lambda \mathbb{R}^n \to T_\Lambda \mathbb{R}^n$ maps $T_x\mathbb{R}^n$ to $T_{f(x)}\mathbb{R}^n$ for each $x \in \Lambda$. Moreover, $Df(E^u_x) = E^u_{f(x)}$ and $Df(E^s_x) = E^s_{f(x)}$.
- 1. and 2. are called hyperbolicity conditions. Notice that λ is a constant value independent of the choices of v and x.

Hyperbolic sets are of particular interest because it is well known that the dynamics of a smooth map f in a hyperbolic set are structurally stable. The statement and proof of this property can be found in [Ano67] and [Mos69] respectively.

Therefore, this section aims to show that the invariant set of any system topologically conjugated to the horseshoe map is hyperbolic. We will postpone this proof to show first the conditions under which this topological conjugation exists.

As we already mentioned, transformations are no longer assumed to be linear. Thus, in the majority of the cases, $f^k(\mathcal{S}) \cap \mathcal{S}$ will not be a union of rectangles. Consequently, it is needed to provide a definition of vertical and horizontal strips that shares the most characteristic properties of the rectangles obtained under the iteration of the linear horseshoe from last section.

Definition 3.7. A vertical curve $x = v(y)$ is a curve satisfying $0 \leq v(y) \leq 1$ and $|v(y_1) - v(y_2)| \leq \mu|y_1 - y_2|$ for $0 \leq y_1 \leq y_2 \leq 1$ and $0 < \mu < 1$.
Analogously a horizontal curve $y = h(x)$ is a curve satisfying $0 \leq h(x) \leq 1$ and $|h(x_1) - h(x_2)| \leq \mu|x_1 - x_2|$ for $0 \leq x_1 \leq x_2 \leq 1$ and $0 < \mu < 1$.

Definition 3.8. Let v_1, v_2, h_1, h_2 be two non-intersecting vertical and horizontal curves respectively. Assuming that $v_1(y) < v_2(y), \forall y \in [0,1]$ and $h_1(x) < h_2(x), \forall x \in [0,1]$, we define a vertical strip V and a horizontal strip H as:

$$V = \{(x,y) : x \in [v_1(y), v_2(y)], \forall y \in [0,1]\}$$

$$H = \{(x,y) : y \in [h_1(x), h_2(x)], \forall x \in [0,1]\}$$

The diameter of a strip is defined as the maximum width it achieves:

$$d(V) = \max_{y \in [0,1]} |v_2(y) - v_1(y)| \qquad d(H) = \max_{x \in [0,1]} |h_2(x) - h_1(x)|$$

The following two lemmas state some properties of the vertical and horizontal strips used in the upcoming proofs. The statements are pretty intuitive and resemble the structure of the linear horseshoe from section 3.1.

Lemma 3.9. If $\{V_k\}_{k \geq 1}$ is a sequence of nested vertical strips such that $V_{k+1} \subset V_k, \forall k \geq 1$ and $\lim_{k \to \infty} d(V_k) = 0$, then $\bigcap_{k=1}^{\infty} V_k$ which will be noted as V_∞ is a vertical curve.

Proof. See section A.3 in Appendix A. □

Remark 3.10. Lemma 3.9 holds with horizontal strips.

Lemma 3.11. A vertical curve $x = v(y)$ and a horizontal curve $y = h(x)$ intersect in precisely one point.

Proof. See section A.4 in Appendix A. □

Therefore, if h is a horizontal curve and v is a vertical curve, there exist a unique point of intersection $p = (x, y)$. With that notation, let us introduce the norms:

$$||u|| = \max_{x \in [0,1]} |u(x)| \qquad ||v|| = \max_{y \in [0,1]} |v(y)| \qquad |p| = |x| + |y|$$

Using those norms, one can bound the distance between points in the intersection of a vertical and horizontal strip in terms of their diameters.

Lemma 3.12. Let h_1, h_2 be two horizontal curves and let v_1, v_2 be two vertical curves such that $p_1 = h_1 \cap v_1, p_2 = h_2 \cap v_2$. Then:

$$|p_2 - p_1| \leq \frac{1}{1-\mu}(||h_2 - h_1|| + ||v_2 - v_1||)$$

Proof. See section A.5 in Appendix A. □

In the following, we consider a map $f : \mathcal{S} \to \mathbb{R}^2$ which we want to be topologically conjugated with the horseshoe map. The next step is to state two hypotheses $\mathcal{H}1$ and $\mathcal{H}2$, relaxing the conditions of a horseshoe. In general, the veracity of $\mathcal{H}2$ is difficult to check. Hence a third hypothesis $\mathcal{H}3$ is added, which, as we shall see, is related to $\mathcal{H}1$ and $\mathcal{H}2$. We closely follow the exposition in [GH13].

$\mathcal{H}1$: Take $I_N = \{1, 2, 3, ..., N\}$ and let H_i, V_i for $i \in I_N$ be disjoint horizontal and vertical strips. Then $f(H_i) = V_i$ for $i \in I_N$. Additionally, the horizontal boundaries of H_i are mapped into the horizontal boundaries of V_i.

$\mathcal{H}2$: f contracts vertical and horizontal strips uniformly. Specifically, there exists a constant $\nu \in (0, 1)$ such that:

$$V \in \bigcup_{i \in I_N} V_i \implies f(V) \cap V_i = \overline{V_i}, \forall i \in I_N$$

$$H \in \bigcup_{i \in I_N} H_i \implies f^{-1}(H) \cap H_i = \overline{H_i}, \forall i \in I_N$$

where V_i is a vertical strip and H_i is a horizontal strip, which in particular are non-empty. Moreover:

$$d(\overline{V_i}) \leq \nu d(V_i) \quad \text{and} \quad d(\overline{H_i}) \leq \nu d(H_i)$$

$\mathcal{H}3$: Assuming that $f \in \mathcal{C}^1$, the third hypothesis is the so called cone criterion. The cone criterion states that for each point x inside a vertical strip V, there exists a cone $S^u = \{(\xi, \eta) : |\xi| < \mu|\eta|\}$ for $0 < \mu < 1$ with vertex x such that $Df(S^u) \subset S^u$. Similarly, for each x inside a horizontal strip H, there exists a cone with vertex x defined as $S^s = \{(\xi, \eta) : |\eta| < \mu|\xi|\}$ for $0 < \mu < 1$ such that $Df^{-1}(S^s) \subset S^s$ and the cones S^u and S^s are disjoint. Furthermore, if we define $Df(\xi_0, \eta_0) = (\xi_1, \eta_1)$ and $Df^{-1}(\xi_0, \eta_0) = (\xi_{-1}, \eta_{-1})$ then:

$$|\eta_1| \geq \frac{1}{\mu}|\eta_0| \quad \text{and} \quad |\xi_{-1}| \geq \frac{1}{\mu}|\xi_0|$$

Remark 3.13. There are some important observations regarding the cone conditions:

1. If $p \in \mathcal{S}$ and S^u is the associated vertical cone with vertex p, then $Df(S^u)$ is a thinner cone with vertex $f(p)$. Similarly if S^s is the associated horizontal cone with vertex p, then $Df^{-1}(S^s)$ is a thinner cone with vertex $f^{-1}(p)$. This geometric approach is represented in Figure 3.4.
2. When $\mathcal{H}3$ holds, then hyperbolicity of Λ can be proved using that E^s_Λ and E^u_Λ from definition 3.5 coincide with the intersection of such cones.
3. Since we are interested in the hyperbolicity around Λ, there is enough with $\mathcal{H}3$ being satisfied in the region $\bigcup_{i,j\in I_N}(V_i \cap H_j)$.

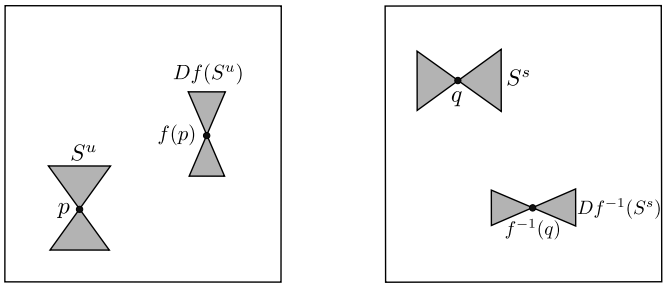

Figure 3.4: Effect of the cone conditions.

The following result presents the main relationship between the three hypotheses. It will be crucial in other proofs because conditions from $\mathcal{H}3$ are more straightforward to check than conditions from $\mathcal{H}2$.

Proposition 3.14. $\mathcal{H}1$ and $\mathcal{H}3$ with $0 < \mu < \frac{1}{2}$ imply $\mathcal{H}2$ with $\nu = \frac{\mu}{1-\mu}$.

Proof. See section A.6 in Appendix A. □

Now we are prepared to state and prove the Theorem establishing the hypotheses granting topological conjugacy of a map f with the shift map. Recall from remark 3.2 that the shift map is topologically conjugated to the horseshoe map. Hence due to topological conjugacy being an equivalence relation, the next theorem grants topological conjugacy between f and the horseshoe map.

Theorem 3.15. Let $f : \mathcal{S} \to \mathbb{R}$ be a homeomorphism satisfying $\mathcal{H}1$ and $\mathcal{H}2$. Then f has an invariant set Λ in which f is topologically equivalent to the shift map σ on Σ, the set of bi-infinite sequences of elements of I_N. In other words, there exists a homeomorphism $h : \Sigma \to \Lambda$ such that $f_{|\Lambda} = h \circ \sigma \circ h^{-1}$. Moreover, if f is a $\mathcal{C}^r$-diffeomorphism with $r \geq 1$ satisfying $\mathcal{H}1$ and $\mathcal{H}3$ with $0 < \mu < \frac{1}{2}$ and it is also true that $|Det(Df)| \leq \frac{1}{2}\mu^{-2}$ and $|Det(Df)|^{-1} \leq \frac{1}{2}\mu^{-2}$, then Λ is a hyperbolic set.

Proof. See section A.7 in Appendix A. □

Chapter 4

The Shilnikov Theorem

The goal of this chapter is to study the richness of dynamics around a homoclinic orbit to a saddle-focus as described by system f_γ in the case $\sigma = \alpha + \lambda > 0$ from section 2.1.3. This dynamics is described by the Shilnikov Theorem, whose proof is deduced from the results in section 2.1 and chapter 3.

First of all, we will gain some intuition on the theorem and set some premises. Take $\delta > 0$ small and an interval (z', z'') satisfying the next conditions:

C.1 $\frac{z''}{z'} = e^{\frac{2\pi\lambda}{\beta}}$. This is to consider exactly one full turn of the spiral generated by the image of a vertical segment in $\mathcal{S}$ by $\mathcal{P}$ as seen in subsection 2.1.3.

C.2 z' and z'' are small enough so that $(\frac{z_1}{z})^{\frac{\alpha}{\lambda}} < \delta, \forall z \in (z', z'')$.

C.3 If $|\theta| < \delta$, then $\mathcal{P}(\theta, z') \notin \Sigma_0$ and $\mathcal{P}(\theta, z'') \notin \Sigma_0$. This guarantees that the end points of the turn of the spiral lay in $\overline{\Sigma_0} \setminus \Sigma_0$, i.e., below the stable invariant manifold.

We will see that under these three assumptions, for each of those intervals (z', z'') there exist sets $\overline{\mathcal{S}} \subset \mathcal{S}$ such that $\mathcal{P}$ is a horseshoe map. These sets are defined as follows:

$$\overline{\mathcal{S}} = \{(r_0, \theta, z) \in \mathcal{S} : z \in (z', z'')\}$$

for (z', z'') verifying the previous conditions. Now that we can identify maps resembling horseshoes, it is essential to understand the difference between the cases $\sigma < 0$ discussed in section 2.2 and the case $\sigma > 0$ discussed here. On the one hand, if $\sigma < 0$, then for small enough values of z, one has that $\overline{\mathcal{S}} \cap \mathcal{P}(\overline{\mathcal{S}}) = \emptyset$ because in this case, $\mathcal{P}$ is a contraction mapping. On the other hand, the intersection between $\mathcal{P}(\overline{\mathcal{S}})$ and $\overline{\mathcal{S}}$ is non-empty for small values of z. This intersection can be formed of either one or two connected components. The differences between the two cases are illustrated in Figure 4.1.

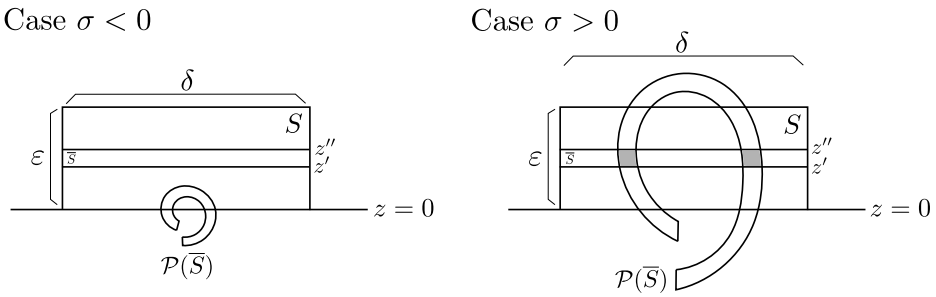

Figure 4.1: Spiral $\mathcal{P}(\overline{\mathcal{S}})$ in the cases $\sigma < 0$ and $\sigma > 0$ and its intersection with $\overline{\mathcal{S}}$ when it is non-empty.

Remark 4.1. If $\sigma > 0$, the Poincaré map $\mathcal{P}$ is expansive, as we saw in subsection 2.1.3. Therefore, there exist a small $z > 0$ such that for every pair of values (z', z'') satisfying **C.1**, **C.2**, **C.3** and $0 < z' < z'' < z$, the set $(\mathcal{P})(\overline{\mathcal{S}}) \cap \overline{\mathcal{S}}$ consists of two connected components.

Those premises establish a suitable setting to state the Shilnikov Theorem, which describes the dynamics of the systems f_γ around the homoclinic orbit of f_{γ_0} when $\sigma > 0$. In [Kuz13], the Theorem is stated in terms of the split function, see 1.2.3. Below, we detail the ideas of the proof in [GH13].

Theorem 4.2. (Shilnikov 1965) Let $\dot{x} = f(x, \gamma)$ be a three-dimensional parametric dynamical system with $f : \mathbb{R}^3 \times \mathbb{R} \to \mathbb{R}^3$ smooth. Assume that f has at $\gamma = \gamma_0$ a homoclinic orbit Γ_0 to a saddle-focus equilibrium x_0 with a real eigenvalue $\lambda > 0$ and two complex eigenvalues $\omega, \overline{\omega}$ with $\omega = \alpha + i\beta$ and $\alpha < 0$. Additionally, assume that $\sigma = \alpha + \lambda > 0$ and $\rho'(\gamma_0) \neq 0$, where ρ is the split function.
Then, the system $\dot{x} = f(x, \gamma)$ has an infinite number of saddle limit cycles in a neighbourhood of $\Gamma_0 \cup \{x_0\}$ for all γ such that $|\rho(\gamma)|$ is sufficiently small.

Proof. First we consider the system $\dot{x} = f(x, \gamma)$ for $\gamma = \gamma_0$. At the end of the proof, we justify that it also holds for sufficiently small values of $|\rho(\gamma)|$. Recall that for $\gamma = \gamma_0$, the system has a homoclinic orbit to the saddle-focus, hence $\rho(\gamma_0)$.

We will prove that for each of the intervals (z', z'') satisfying **C.1**, **C.2**, **C.3** and such that z', z'' are sufficiently small so that $\mathcal{P}(\overline{\mathcal{S}}) \cap \overline{\mathcal{S}}$ is composed of two connected components as seen in remark 4.1, the Poincaré map $\mathcal{P}$ has a horseshoe in $\overline{\mathcal{S}} = \{(r_0, \theta, z) \in \mathcal{S} : z \in (z', z'')\}$. We shall use the results from Chapter 3. The main idea is to check that hypotheses $\mathcal{H}1$ and $\mathcal{H}3$ hold, hence by Prop 3.14 hypothesis $\mathcal{H}2$ is also satisfied, and consequently Theorem 3.15 can be applied. It follows that we obtain by construction a Cantorian hyperbolic set in $\overline{\mathcal{S}}$, i.e. a

closed perfect and totally disconnected set, in which the dynamics is conjugated to the one of the shift map. In particular, such a set contains saddle periodic orbits of $\mathcal{P}$ for any large enough period.

First of all, by differentiability with respect to initial conditions, since f is smooth, its flux is also smooth. Additionally, the tubular flux theorem, necessary to define $\mathcal{P}$, gives a $\mathcal{C}^1$ conjugacy. Consequently, $\mathcal{P}$ is a smooth map. In subsection 2.1.3 we saw that vertical lines in $\overline{\mathcal{S}} \subset \mathcal{S}$ are mapped by $\mathcal{P}$ into pieces of spiral in Σ_0 that intersect $\overline{\mathcal{S}}$ in vertical curves, as represented in the second picture of Figure 4.1. Therefore, by continuity, horizontal strips in $\overline{\mathcal{S}}$ are mapped into vertical strips in $\overline{\mathcal{S}}$ by $\mathcal{P}$, which indicates that hypothesis $\mathcal{H}1$ is satisfied.

It just remains to prove that $\mathcal{P}$ satisfies hypothesis $\mathcal{H}3$. Let us define the projection $\Pi_{XY} : \mathbb{R}^2 \times \{z_1\} \to \mathbb{R}^2$ defined by $\Pi_{XY}(x, y, z_1) = (x, y)$. With that projection, we can define the inner and outer transition to $2-$dimensional maps $\overline{\psi_1} = \Pi_{XY} \circ \psi_1 \circ C^{-1} \circ \Pi^{-1}$, from Σ_0 to Σ_1 and $\overline{\psi_2} = \Pi \circ C \circ \psi_2 \circ \Pi_{XY}^{-1}$, from Σ_1 to Σ_0. Therefore, one can express the Poincaré map as $\mathcal{P} = \overline{\psi_2} \circ \overline{\psi_1}$. Using elementary trigonometric identities, one deduces from (2.4) that:

$$\overline{\psi_1} \begin{pmatrix} \theta \\ z \end{pmatrix} = \begin{pmatrix} r_0 \left(\frac{z_1}{z}\right)^{\frac{\alpha}{\lambda}} \cos\left(\theta + \kappa(z)\right) \\ r_0 \left(\frac{z_1}{z}\right)^{\frac{\alpha}{\lambda}} \sin\left(\theta + \kappa(z)\right) \end{pmatrix} \tag{4.1}$$

where $k(z)$ is defined in (2.3). The differential matrix of $\overline{\psi_1}$ can be expressed as a product of simpler matrices as follows:

$$D\overline{\psi_1} \begin{pmatrix} \theta \\ z \end{pmatrix} = r_0 (\frac{z_1}{z})^{\frac{\alpha}{\lambda}} \begin{pmatrix} \cos\left(\kappa(z)\right) & -\sin\left(\kappa(z)\right) \\ \sin\left(\kappa(z)\right) & \cos\left(\kappa(z)\right) \end{pmatrix} \begin{pmatrix} -\sin\left(\theta\right) & \frac{-\alpha\cos\left(\theta\right)+\beta\sin\left(\theta\right)}{\lambda z} \\ \cos\left(\theta\right) & \frac{-\alpha\sin\left(\theta\right)-\beta\cos\left(\theta\right))}{\lambda z} \end{pmatrix}$$

Let us define $A = D\overline{\psi_2}(\overline{\psi_1}(\theta, z))$, and two auxiliary matrices:

$$B = r_0 z_1^{\frac{\alpha}{\lambda}} A \begin{pmatrix} \cos\left(\kappa(z)\right) & -\sin\left(\kappa(z)\right) \\ \sin\left(\kappa(z)\right) & \cos\left(\kappa(z)\right) \end{pmatrix} \qquad C = \begin{pmatrix} -\sin\left(\theta\right) & \frac{-\alpha\cos\left(\theta\right)+\beta\sin\left(\theta\right)}{\lambda} \\ \cos\left(\theta\right) & \frac{-\alpha\sin\left(\theta\right)-\beta\cos\left(\theta\right)}{\lambda} \end{pmatrix}$$

With those definitions, one can check that:

$$D(\mathcal{P})(\theta, z) = D(\overline{\psi_2} \circ \overline{\psi_1})(\theta, z) = A \cdot D\overline{\psi_1}(\theta, z) = z^{-\left(\frac{\alpha}{\lambda}+1\right)} BC \begin{pmatrix} z & 0 \\ 0 & 1 \end{pmatrix}$$

We are interested in the eigenvalues and eigenvectors of that matrix evaluated at points from $\mathcal{P}(\overline{\mathcal{S}}) \cap \overline{\mathcal{S}}$ for a certain $\overline{\mathcal{S}}$ defined as specified above. This last decomposition of $D(\mathcal{P})$ into products of matrices is useful to justify that all the

eigenvalues and eigenvectors are almost uniform for points in that region. To see that, we must study some of the properties of the matrices B and C.

One can check that $Det(C) = \frac{\alpha}{\lambda} \neq 0$ because we are assuming that $\sigma > 0$, hence C is nonsingular. Moreover, the points in $\mathcal{P}(\overline{\mathcal{S}}) \cap \overline{\mathcal{S}}$ are such that $|\theta| < \delta$ for a small value $\delta > 0$ (recall that θ is the angle of the cylindrical coordinates centered at the origin, see the second picture from Figure 4.1). Consequently, $\sin(\theta) \approx \theta$ and $\cos(\theta) \approx 1$ so we can conclude that C is approximately constant in both of the connected components of $\mathcal{P}(\overline{\mathcal{S}}) \cap \overline{\mathcal{S}}$.

On the other hand, assuming that $\mathcal{P}(\overline{\mathcal{S}}) \cap \overline{\mathcal{S}}$ is the union of two connected components, the images under $\overline{\psi_1}$ of points from each of those components differ by approximately $\theta = \pi$. Thus, matrix B is approximately multiplied by $-Id$, playing no role on the pertinent properties of the eigenvalues and eigenvectors.

Therefore, choosing z' and z'' sufficiently small, each of the connected components of $\mathcal{P}(\overline{\mathcal{S}}) \cap \overline{\mathcal{S}}$ has area close to zero and the coefficients of $D\mathcal{P}$ are almost constant in each of those regions. Now, for an arbitrary point in one of those connected components, denote the constant matrices B and C as $B = (b_{ij})$ and $C = (c_{ij})$ for $i, j \in \{1, 2\}$. Observe that taking the limit as z tends to 0:

$$\begin{aligned} \lim_{z\to 0} D\mathcal{P}(\theta, z) &= \lim_{z\to 0} z^{-(\frac{\alpha}{\lambda}+1)} \begin{pmatrix} b_{11} & b_{12} \\ b_{21} & b_{22} \end{pmatrix} \begin{pmatrix} c_{11} & c_{12} \\ c_{21} & c_{22} \end{pmatrix} \begin{pmatrix} 0 & 0 \\ 0 & 1 \end{pmatrix} = \\ &= \lim_{z\to 0} z^{-(\frac{\alpha}{\lambda}+1)} \begin{pmatrix} 0 & b_{11}c_{12} + b_{12}c_{22} \\ 0 & b_{21}c_{12} + b_{22}c_{22} \end{pmatrix} \end{aligned} \tag{4.2}$$

Since $\sigma > 0$, the value of $\mu = \lim_{z\to 0} z^{-(\frac{\alpha}{\lambda}+1)}$ tends to infinity as z tends to 0, hence that matrix has 0 and $\mu(b_{21}c_{12} + b_{22}c_{22})$ as eigenvalues, which are separated for small values of z. In particular, that matrix is diagonalizable: there exist a nonsingular matrix P and a diagonal matrix D such that, for small values of z, $D\mathcal{P}(\theta, z) = PDP^{-1}$. As we explained, the coefficients of this matrix may vary slightly inside each connected component of $\mathcal{P}(\overline{\mathcal{S}}) \cap \overline{\mathcal{S}}$, but the Bauer-Fike theorem guarantees that the eigenvalues of a matrix with similar coefficients are approximately the same. Here we will state this theorem, see proof in [BF60].

Theorem 4.3. Let $A \in \mathbb{C}^{n\times n}$ be a diagonalizable matrix, i.e., there exist a nonsingular matrix $P \in \mathbb{C}^{n\times n}$ and a diagonal matrix $D \in \mathbb{C}^{n\times n}$ such that $A = PDP^{-1}$. Given a matrix $E \in \mathbb{C}^{n\times n}$, define $B = A - E$ and let μ be an eigenvalue of B, then there exists an eigenvalue λ of A such that:

$$|\lambda - \mu| \leq \kappa_p(P)||E||_p$$

where $||\cdot||_p$ is the matrix p-norm in $\mathbb{C}^{n\times n}$ and $\kappa_p(P) = ||P||_p||P^{-1}||_p$ is the condition number of P in that norm.

Therefore, returning to our case, for small enough values of z, the differential matrix $D\mathcal{P}(\theta, z)$ of a point in one of the connected components of $\mathcal{P}(\overline{\mathcal{S}}) \cap \overline{\mathcal{S}}$ has eigenvalues arbitrarily close to the eigenvalues of the differential matrix of another point in the same connected component. The reason is that the coefficients of the perturbation matrix E from Theorem 4.3 becomes arbitrarily small when z tends to zero. Consequently, the distance between eigenvalues decreases by an unbounded amount. In consequence, we can work with the eigenvalues and eigenvectors of a point in one of the connected components of $\mathcal{P}(\overline{\mathcal{S}}) \cap \overline{\mathcal{S}}$ and assume that the eigenvalues and eigenvectors of other points from the same connected component are to all intents and purposes the same.

From equation (4.2), the eigenvectors of 0 and $\mu(b_{21}c_{12} + b_{22}c_{22})$ are $(1, 0)$ and $(b_{11}c_{12} + b_{12}c_{22}, b_{21}c_{12} + b_{22}c_{22})$ which set the direction of the stable and unstable spaces of the considered point respectively. The slope of the second eigenvector is

$$m = \frac{b_{21}c_{12} + b_{22}c_{22}}{b_{11}c_{12} + b_{12}c_{22}} \in \mathbb{R} \cup \{\infty\}$$

Since eigenvectors of different eigenvalues are linearly independent, taking points $(\theta, z) \in \mathcal{P}(\overline{\mathcal{S}}) \cap \overline{\mathcal{S}}$ with z sufficiently small so that the eigenvalue $\mu(b_{21}c_{12} + b_{22}c_{22})$ is bounded away from 0, one has that the slope m is also bounded away from 0, which is the slope of the eigenvector $(1, 0)$. Figure 4.2 shows that the fact that $\mathcal{P}(\overline{\mathcal{S}}) \cap \overline{\mathcal{S}}$ is the union of two connected components for small values of z as seen in Remark 4.1, is directly related to the value of the difference between the slopes of the eigenvectors of a point $(\theta, z) \in \mathcal{P}(\overline{\mathcal{S}}) \cap \overline{\mathcal{S}}$.

The different directions of the eigenvectors are used to construct a cone field and verify the hyperbolicity of the restriction of $\mathcal{P}$ on the invariant set. We can choose for every point in $\mathcal{P}(\overline{\mathcal{S}}) \cap \overline{\mathcal{S}}$ two disjoint cones centered at that point. Denote the one situated around $(1, 0)$ by S^s and the other one situated around $\mu(b_{21}c_{12} + b_{22}c_{22})$ by S^u . As it was explained in remark 3.13, having cones defined in this region is enough for what we expect to prove.

Notice that those cones converge to a line under iteration by $D(\mathcal{P})$. It is clear that $|\theta|$ converges to 0 as z tends to 0, hence S^u tends to $(0, 1)$. To see the convergence of S^s, fix a value θ_0 such that $|\theta_0| < \delta$ and define the points $P_1 = (\psi_1 \circ C^{-1})(r_0, \theta_0, z') \in \Sigma_1$ and $P_2 = (\psi_1 \circ C^{-1})(r_0, \theta, z'') \in \Sigma_1$ that lay in the spiral $C_S = \{\tilde{\psi}_1(z) : 0 < z < \epsilon\} \subset \Sigma_1$ for $\theta = \theta_0$ fixed. Let L_1 and L_2 be the lines defined

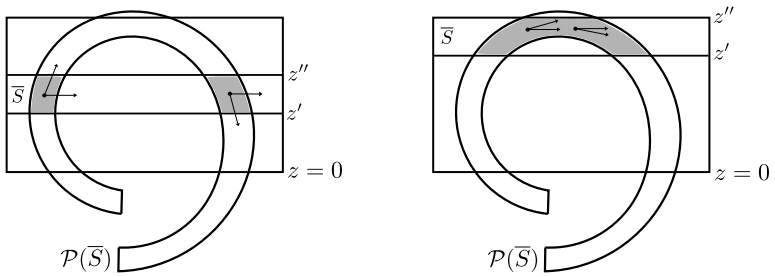

Figure 4.2: Eigenvectors when $\mathcal{P}(\overline{\mathcal{S}})$ is composed of two and one connected components. In the first case, the difference between the slopes of the eigenvectors is bounded away from 0, whereas in the second case, both eigenvectors have slopes close to 0 in a region on the top of the spiral.

by $\{P_1, (0,0,z_1)\} \subset L_1$ and $\{P_2, (0,0,z_1)\} \subset L_2$ as shown in Figure 4.3. Repeating this construction as z' and z'' tend to 0, the angle between L_1 and L_2 converges to 0. To see that, we compute the difference between the arguments of P_2 and P_1 given in (4.1). Additionally, we will use the hypothesis **C.1**:

$$\left| r_0 \left(\frac{z_1}{z''}\right)^{\frac{\alpha}{\lambda}} \cos\left(\theta_0 + \frac{\beta}{\lambda}\log\left(\frac{z_1}{z''}\right)\right) - r_0 \left(\frac{z_1}{z'}\right)^{\frac{\alpha}{\lambda}} \cos\left(\theta_0 + \frac{\beta}{\lambda}\log\left(\frac{z_1}{z'}\right)\right)\right| \leq$$

$$\leq r_0 z_1^{\frac{\alpha}{\lambda}} \left(\frac{1}{z''^{\frac{\alpha}{\lambda}}} + \frac{1}{z'^{\frac{\alpha}{\lambda}}}\right) = r_0 z_1^{\frac{\alpha}{\lambda}} \left(\frac{1}{z''^{\frac{\alpha}{\lambda}}} + \frac{e^{\frac{2\pi\alpha}{\beta}}}{z''^{\frac{\alpha}{\lambda}}}\right) = \frac{r_0 z_1^{\frac{\alpha}{\lambda}} \left(1 + e^{\frac{2\pi\alpha}{\beta}}\right)}{z''^{\frac{\alpha}{\lambda}}}$$

Since $\frac{\alpha}{\lambda} < 0$, the limit as z' and z'' tend to 0 of the difference between the angles of L_1 and L_2 is 0, i.e., L_1 and L_2 converge to a line $L \subset \Sigma_1$ passing through $Q = (0,0,z_1)$. If $v \in \mathbb{R}^3$ is the direction vector of L, then S^s converges to the line $D\psi_2(v)$, which is tangent to Σ_0 and contains the point $(r_0, 0, 0)$, which is expressed in cylindrical coordinates. Since the disjoint cones around the eigenvectors tend to a limit, we conclude that for any small pair of cones, hypothesis $\mathcal{H}3$ is satisfied as we wanted to prove.

By Prop 3.14, we know that $\mathcal{H}2$ is also satisfied and consequently all the hypotheses of Theorem 3.15 hold. Consequently, the Poincaré map $\mathcal{P}$ associated to the system $\dot{x} = f(x, \gamma)$ and defined on the set $\mathcal{P}(\overline{\mathcal{S}}) \cap \overline{\mathcal{S}}$ is topologically conjugated to the horseshoe map. Moreover, its invariant set $\Lambda \subset \mathcal{P}(\overline{\mathcal{S}}) \cap \overline{\mathcal{S}}$ is hyperbolic, and since hyperbolic sets are structurally stable, systems $\dot{x} = f(x, \gamma)$ such that $|\rho(\gamma)|$ is sufficiently small, contain an invariant set preserving the dynamics of Λ.

Additionally, we can prove that there exist an infinite amount of horseshoes in $\mathcal{S}$. Let (z', z'') be a pair of values satisfying **C.1**, **C.2**, **C.3** and such that z' and z'' are

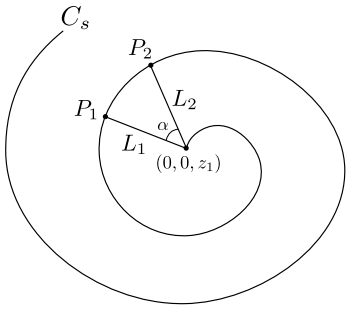

Figure 4.3: We illustrate the angle α between the lines L_1 and L_2 in Σ_1. Recall that α tends to 0 as z tends to 0. See text for details.

small enough for $\mathcal{P}(\overline{\mathcal{S}}) \cap \overline{\mathcal{S}}$ to be the union of two connected components, where $\overline{\mathcal{S}} = \{(r_0, \theta, z) \in \mathcal{S} : z \in (z', z'')\}$. From 4.1 one deduces that when z tends to 0, the spiral $\mathcal{P}(\mathcal{S})$ spirals infinitely many times around $(r_0, 0, 0)$. Therefore, there exists a value z_0' such that $0 < z_0' < z'$ and (z_0', z') satisfies **C.1**, **C.2** and **C.3**. We just saw that under those hypotheses, $\mathcal{P}$ has a horseshoe in $\mathcal{P}(\overline{\mathcal{S}_0}) \cap \overline{\mathcal{S}_0}$, where $\overline{\mathcal{S}_0} = \{(r_0, \theta, z) \in \mathcal{S} : z \in (z_0', z')\}$. This procedure can be repeated an infinite number of times, one for each full turn of the spiral $\mathcal{P}(\mathcal{S})$ closer to its centre $(r_0, 0, 0)$. The situation is sketched in Figure 4.4.

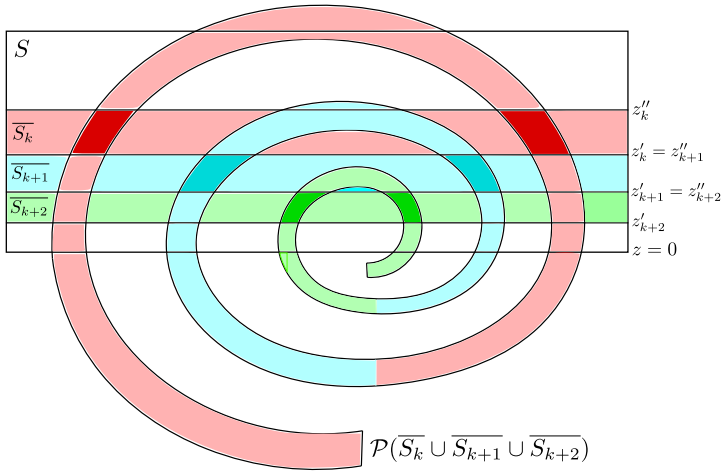

Figure 4.4: In this picture we show three horseshoes and the location of their corresponding hyperbolic sets. As explained in the text, we could continue illustrating smaller horseshoes closer to the centre of the spiral.

By Theorem 3.3, each of the horseshoes of $\mathcal{P}$ has an infinite number of saddle periodic orbits of arbitrarily long period in its hyperbolic invariant set Λ. Therefore, as

$\mathcal{P}$ is a Poincaré map, the periodic orbits correspond to saddle limit cycles of an arbitrarily long period of the original system f_γ in a neighbourhood of $\Gamma_0 \cup \{x_0\}$. $\square$

Notice that throughout the proof, it was not used that the homoclinic orbit breaks after perturbing the parameter of the system. Therefore, the chaotic dynamics hold even under perturbations preserving the homoclinic orbit. Nonetheless, it was proven in Chapter 1 that the homoclinic orbit can not be preserved in all systems sufficiently $\mathcal{C}^1 - close$ to $f_{\gamma_0}(x)$. Consequently, the chaotic behaviour of a parametric system containing a homoclinic orbit to a saddle-focus is unavoidably linked to the appearance of a bifurcation when the parameter is slightly varied. This completes the study of the complex dynamics of a Shilnikov system in the case $\sigma > 0$ around the homoclinic orbit.

Chapter 5

Illustration of the Shilnikov bifurcation scenarios

This chapter aims to study and develop the appropriate numerical methods to illustrate the homoclinic bifurcations to a saddle-focus equilibrium in the cases $\sigma > 0$ and $\sigma < 0$, where σ denotes the saddle value of the saddle-focus. Moreover, we will discuss numerically some properties that could not be treated in Chapter 2 with analytical techniques without considering a particular system.

First of all, we need a system of differential equations in dimension 3 containing a homoclinic orbit to a saddle-focus equilibrium. Currently, there are some known and well-studied equations modelling systems that manifest Shilnikov bifurcations. Some examples are the Chua circuit [CKM86] which is a simple electronic circuit exhibiting chaotic behaviour, and the FitzHugh-Nagumo model of the nerve impulse propagation along an axon (see [Fit61] and [NAY62]).

Instead, we obtain our $3-$dimensional system following [GL96] to build dynamical systems containing homoclinic orbits from lower dimensional ones. We illustrate both cases $\sigma < 0$ and $\sigma > 0$ with similarly constructed examples.

5.1 Model derivation

In this section, we construct a $3-$dimensional system of differential equations containing a homoclinic orbit to a hyperbolic point from a $2-$dimensional system satisfying certain hypotheses. The method introduced in this section is far more useful because we can use it to obtain systems of higher dimensions containing homoclinic orbits to hyperbolic equilibrium.

Take a $2-$dimensional system with a parameter $\mu \in \mathbb{R}$ having the next structure:

$$\dot{x} = Ax + F(x,\mu) = \begin{pmatrix} a_{00} & a_{01} \\ a_{10} & a_{11} \end{pmatrix} \begin{pmatrix} x_1 \\ x_2 \end{pmatrix} + \begin{pmatrix} F_1(x,\mu) \\ F_2(x,\mu) \end{pmatrix} \tag{5.1}$$

where $F(x,\mu)$ is a smooth function that contains only non-linear terms, that is, $F_1(0,\mu) = F_2(0,\mu) = 0, \forall \mu \in \mathbb{R}$. Moreover, assume that A is a constant matrix, $x_0 = 0$ is a hyperbolic fixed point, and that the following two statements hold:

1. There exists a value $\mu_H \in \mathbb{R}$ in which the system has a homoclinic orbit $x_H(t)$ to x_0, and it does not have any other homoclinic orbit at any parameter value $\mu \in (\mu_H - \epsilon, \mu_H + \epsilon) \setminus \{\mu_H\}$, for small values of $\epsilon > 0$.
2. The eigenvalues of A are $\nu, \lambda \in \mathbb{R}$ with $\nu < 0 < \lambda$ and $x_H(t)$ is tangent to the subspaces generated by e_s the eigenvector of eigenvalue ν and e_u the eigenvector of eigenvalue λ.

In particular, if $\nu + \lambda \neq 0$, this system has saddle-node homoclinic orbit at $\mu = 0$. Examples of systems satisfying those hypotheses are easy to find. Consequently, those conditions are not very restrictive. This system works as a seed, and now we will modify it and add a new equation to obtain a $3-$dimensional system with the desired properties.

Recalling that A and A^T have the same eigenvalues, let $e_s^\dagger$ and $e_u^\dagger$ be the eigenvectors of eigenvalues ν and λ of A^T. If we denote their coordinates as $e_s^\dagger = (e_{s\restriction x}^\dagger, e_{s\restriction y}^\dagger)^T$ and $e_u^\dagger = (e_{u\restriction x}^\dagger, e_{u\restriction y}^\dagger)^T$, then by definition it is satisfied that:

$$A^T e_s^\dagger = \nu e_s^\dagger \iff \begin{pmatrix} a_{00} e_{s\restriction x}^\dagger + a_{10} e_{s\restriction y}^\dagger \\ a_{01} e_{s\restriction x}^\dagger + a_{11} e_{s\restriction y}^\dagger \end{pmatrix} = \begin{pmatrix} \nu e_{s\restriction x}^\dagger \\ \nu e_{s\restriction y}^\dagger \end{pmatrix} \tag{5.2}$$

$$A^T e_u^\dagger = \lambda e_u^\dagger \iff \begin{pmatrix} a_{00} e_{u\restriction x}^\dagger + a_{10} e_{u\restriction y}^\dagger \\ a_{01} e_{u\restriction x}^\dagger + a_{11} e_{u\restriction y}^\dagger \end{pmatrix} = \begin{pmatrix} \lambda e_{u\restriction x}^\dagger \\ \lambda e_{u\restriction y}^\dagger \end{pmatrix} \tag{5.3}$$

Moreover, taking the transpose of every side from the definition of being eigenvectors, one has that:

$$\left(e_s^\dagger\right)^T A = \nu \left(e_s^\dagger\right)^T \quad \text{and} \quad \left(e_u^\dagger\right)^T A = \lambda \left(e_u^\dagger\right)^T \tag{5.4}$$

Additionally, assume that the vectors are normalized so that $e_s^\dagger \cdot e_s = e_u^\dagger \cdot e_u = 1$. The following orthogonality property will also be required for later computations.

Lemma 5.1. Let u be an eigenvector of eigenvalue λ of A, and let v be an eigenvector of eigenvalue μ of A, with $\lambda \neq \mu$. Then, $\langle v, u\rangle = 0$, where $\langle \cdot, \cdot \rangle$ is an inner product defined by $\langle v, u\rangle = v^T u$.

Proof. By definition, $Au = \lambda u$ and $v^T A = \mu v^T$. Therefore:

$$\lambda\langle v, u\rangle = \langle v, \lambda u\rangle = \langle v, Au\rangle = v^T Au = \left(v^T Au\right)^T =$$
$$= \langle u, A^T v\rangle = \langle u, (v^T A)^T\rangle = \langle u, (\mu v^T)^T\rangle = \mu\langle u, v\rangle$$

Since $\langle u, v\rangle = \langle v, u\rangle$, it should be $\lambda = \mu$, but that is not possible by hypothesis. Consequently, it must be $\langle u, v\rangle = \langle v, u\rangle = 0$. □

Now, consider the following $3-$dimensional system which is an extension of the system (5.1):

$$\begin{cases} \dot{x} = Ax - ze_s + F(x, \mu) \\ \dot{z} = \epsilon(e_s^\dagger x) + \nu z \end{cases}$$

Denote as $X_{\mu,\epsilon}(x_1, x_2, z)$ the vector field determining that system. The current goal is to see that it contains a homoclinic orbit to a hyperbolic point for certain values of μ and ϵ. To do that, it is convenient to express the system in coordinates:

$$\begin{pmatrix} \dot{x_1} \\ \dot{x_2} \\ \dot{z} \end{pmatrix} = \begin{pmatrix} a_{00}x_1 + a_{01}x_2 - ze_{s\restriction x} + F_1(x, \mu) \\ a_{10}x_1 + a_{11}x_2 - ze_{s\restriction y} + F_2(x, \mu) \\ \epsilon(e_{s\restriction x}^\dagger x_1 + e_{s\restriction y}^\dagger x_2) + \nu z \end{pmatrix} \tag{5.5}$$

It is clear that the origin is an equilibrium of the system for all values of μ and ϵ, i.e., $X_{\mu,\epsilon}(0, 0, 0) = 0, \forall \mu, \epsilon \in \mathbb{R}$. To study its stability, we need to compute the eigenvalues of $DX_{\mu,\epsilon}(0)$, but it is an elaborate task with those coordinates. Therefore, we will express the system (5.5) in the coordinate system (x_u, x_s, z), where $x = x_s \cdot e_s + x_u \cdot e_u$. Multiplying this last equality by $e_s^\dagger$ and $e_u^\dagger$ separately, and applying some of the shown properties and relations between the left and right eigenvalues, one obtains the next two equalities:

$$\begin{aligned} x_u &= x_1 e_{u\restriction x}^\dagger + x_2 e_{u\restriction y}^\dagger \\ x_s &= x_1 e_{s\restriction x}^\dagger + x_2 e_{s\restriction y}^\dagger \end{aligned} \tag{5.6}$$

Now, taking the derivatives with respect to t in both equations from (5.6) and expressing the result in an appropriate manner, one can use lemma 5.1 and equations (5.2) and (5.3) to obtain the next equalities:

$$\begin{aligned}\dot{x_u} &= \dot{x_1} \cdot e^{\dagger}_{u\restriction x} + \dot{x_2} \cdot e^{\dagger}_{u\restriction y} = \\ &= x_1(\lambda_1 e^{\dagger}_{u\restriction x}) + x_2(\lambda_1 e^{\dagger}_{u\restriction y}) - z(e_s \cdot e^{\dagger}_u) + F(x,\mu) \cdot e^{\dagger}_u = \\ &= \lambda x_u + F(x,\mu) \cdot e^{\dagger}_u\end{aligned}$$

$$\begin{aligned}\dot{x_s} &= \dot{x_1} \cdot e^{\dagger}_{s\restriction x} + \dot{x_2} \cdot e^{\dagger}_{s\restriction y} = \\ &= x_1(\nu e^{\dagger}_{s\restriction x}) + x_2(\nu e^{\dagger}_{s\restriction y}) - z(e_s \cdot e^{\dagger}_s) + F(x,\mu) \cdot e^{\dagger}_s = \\ &= \nu x_s - z + F(x,\mu) \cdot e^{\dagger}_s\end{aligned}$$

The third equation follows from the second equality in (5.6):

$$\dot{z} = \epsilon(e^{\dagger}_{s\restriction x} x_1 + e^{\dagger}_{s\restriction y} x_2) + \nu z = \epsilon x_s + \nu z$$

In conclusion, system (5.5) in coordinates (x_u, x_s, z) reads:

$$\begin{cases} \dot{x_u} = \lambda x_u + F(x,\mu) \cdot e^{\dagger}_u \\ \dot{x_s} = \nu x_s - z + F(x,\mu) \cdot e^{\dagger}_s \\ \dot{z} = \epsilon x_s + \nu z \end{cases}$$

Recalling that $F(x,\mu)$ contains non-linear terms, it is easy to see that in these coordinates, the differential matrix of that vector field at the origin is

$$DX_{\mu,\epsilon}(0) = \begin{pmatrix} \lambda & 0 & 0 \\ 0 & \nu & -1 \\ 0 & \epsilon & \nu \end{pmatrix}$$

One can check that the eigenvalues of that matrix are $\lambda, \nu + \sqrt{-\epsilon}$ and $\nu - \sqrt{-\epsilon}$. Therefore, the origin is a saddle-node equilibrium if $\epsilon \leq 0$, and it is a saddle-focus equilibrium if $\epsilon > 0$. Now, we want to study for which values of μ and ϵ, the system determined by the vector field $X_{\mu,\epsilon}$ has a homoclinic orbit to the origin. Notice that if $\epsilon = z = 0$ in the $3-$dimensional system that we constructed, one obtains the original $2-$dimensional system (5.1) that has by hypothesis a homoclinic orbit at $\mu = \mu_H$. Therefore, on the plane of parameters with coordinates (ϵ, μ), the $3-$dimensional system $X_{\mu_H,0}$ associated to the point $(0, \mu_H)$ has a homoclinic orbit to the origin, which is a saddle-node equilibrium because $\epsilon = 0$.

In general, if X_{μ_0,ϵ_0} has a homoclinic orbit to the origin, then by continuation one expects to have a curve of parameters γ_H in the plane (ϵ, μ) for which the system $X_{\mu,\epsilon}$ has a homoclinic orbit to the origin. Numerical experiments in sections 5.2 and 5.3.2 suggest that there are different curves according to the number of turns

that the homoclinic orbit performs.

Around the parameters (ϵ, μ) for which we have homoclinic orbits, the one parametric system X_{μ,ϵ_0} experiences a Shilnikov bifurcation. Notice that the saddle value $\sigma = \lambda + \mu$ is totally determined by the original $2-$dimensional system, hence small perturbations there, may cause a simple system with $\sigma < 0$ to become into a complicated system with $\sigma > 0$ or vice versa.

5.1.1 Particular example

Based on an example from [GH13], we consider the following $2-$dimensional system of differential equations:

$$\dot{x} = A_{\pm}x + F(x,\mu) = \begin{pmatrix} 0 & 1 \\ 1 & \delta \end{pmatrix} \begin{pmatrix} x_1 \\ x_2 \end{pmatrix} + \begin{pmatrix} 0 \\ \mu x_1 x_2 - x_1^2 \end{pmatrix} \tag{5.7}$$

There, $\delta \in \{-1, +1\}$ and $\mu \in \mathbb{R}$. As seen in section 5.1, all the useful information to extend this system to an appropriate $3-$dimensional system lays in the eigenvalues and eigenvectors of $A_{\pm}$. This system satisfies the conditions imposed on (5.1). In particular, for $\delta = 1$ we see in Figure 5.1 that it presents a homoclinic bifurcation at the origin with critical value $\mu_0 \approx -1.1534765$. As seen in section 5.1, this value of μ is important because for small values of $\epsilon > 0$, the $3-$dimensional system that we will construct from (5.7) should have by continuation a homoclinic orbit to the origin at least for a value μ close to μ_0.

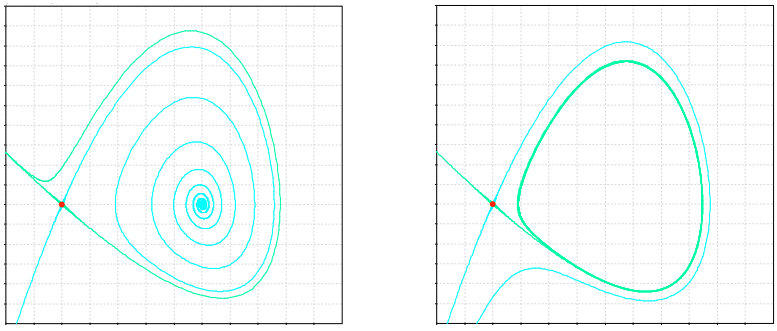

Figure 5.1: We illustrate in the region $[-0.4, 2] \times [-0.6, 1] \subset \mathbb{R}^2$ the appearance of a limit cycle in the $2-$dimensional homoclinic bifurcation of the system (5.7) with $\delta = 1$ as the parameter μ is varied around the critical value $\mu_0 \approx -1.1534765$. The green and blue curves are the stable and unstable manifold of the origin respectively. We used PPlane [Pol] for the illustrations in this figure.

Denote as $\varphi = \frac{1+\sqrt{5}}{2}$ the golden ratio. If $\delta = 1$, one can check that $Spec(A_+) = \{\lambda_1, \nu_1\}$, where $\lambda_1 = \varphi > 0$ and $\nu_1 = 1 - \varphi < 0$. The corresponding eigenvectors are $e_{u,1} = \frac{1}{\sqrt{1+\varphi^2}}(\varphi - 1, 1)^T$ and $e_{s,1} = \frac{1}{\sqrt{1+\varphi^2}}(-\varphi, 1)^T$. Similarly, if $\delta = -1$, then $Spec(A_-) = \{\lambda_{-1}, \nu_{-1}\}$, where $\lambda_{-1} = \varphi - 1$, $\nu_{-1} = -\varphi$ and the corresponding eigenvectors are $e_{u,-1} = (\varphi, 1)^T$ and $e_{s,-1} = (1 - \varphi, 1)$ respectively. Now, depending on the value of δ, one has two $3-$dimensional systems with the structure seen in section 5.1:

$$\begin{cases} \dot{x} = A_\pm x - z e_{s,\delta} + F(x, \mu) \\ \dot{z} = \epsilon(e_{s,\delta} x) + \nu_\delta z \end{cases} \tag{5.8}$$

Notice that in this case $A_\pm A_\pm^T = A_\pm^T A_\pm$ and hence $e_{s,\delta} = e_{s,\delta}^\dagger$ and $e_{u,\delta} = e_{u,\delta}^\dagger$. Denoting the vector field determining that system as $X_{\mu,\epsilon,\delta}$, we saw that $\forall \delta \in \{-1, +1\}$ one has that $Spec(DX_{\mu,\epsilon,\delta}(0)) = \{\lambda_\delta, \nu_\delta \pm \sqrt{-\epsilon}\}$. Since $\lambda_1 + \nu_1 = 1 > 0$ and $\lambda_{-1} + \nu_{-1} = -1 < 0$, we deduce that for strictly positive values of ϵ, the system $X_{\mu,\epsilon,-1}$ has a simple Shilnikov bifurcation with negative saddle value, and the system $X_{\mu,\epsilon,1}$ has a Shilnikov bifurcation with positive saddle value, i.e., presenting the chaotic behaviour studied in Chapter 4. These are the two systems that we will use in the next sections.

5.2 Illustration of homoclinic orbits

Fix a value $\epsilon_0 > 0$ and assume that $X_{\mu,\epsilon_0,1}$ has a homoclinic orbit Γ_0 to the origin at $\mu = \mu_0$. As we explained, this system exhibits a Shilnikov bifurcation with critical value $\mu = \mu_0$ and saddle value $\sigma > 0$. Moreover, by Theorem 4.2 this system has an infinite number of saddle-limit cycles in a neighbourhood of Γ_0 for values of μ close to μ_0.

Preserving the notation from Chapter 2 , we saw in section 2.1.2 that the flight time from Σ_0 to Σ_1 of a point $z \in \Sigma_0$ is $t(z) = \frac{1}{\lambda} \log\left(\frac{z_1}{z}\right)$. Therefore, $\lim_{z \to 0} t(z) = \infty$. Since the limit cycles given by Theorem 4.2 lay in a tubular neighbourhood of Γ_0, they must intersect Σ_0 and Σ_1 in points $P_0 \in \Sigma_0$ and $P_1 \in \Sigma_1$. As said, the flight time increases as P_0 is chosen closer to the plane $z = 0$. In other words, the period of the limit cycles in a tubular neighbourhood of Γ_0 tends to infinity as the distance from the limit cycle to the plane $z = 0$ tends to 0. In particular, the limit cycles tend to the homoclinic orbit as z tends to zero.

We are particularly interested in the computation of Γ_0 to illustrate the bifurcation as μ is varied around μ_0. To do that, we will use the system (5.8) when $\delta = 1$ for

fixed values of $\epsilon \geq 0$, that is expressed in Cartesian coordinates (x, y, z) as:

$$X_{\mu,\epsilon,1}(x,y,z) : \begin{cases} \dot{x} = y + \frac{\varphi}{\sqrt{1+\varphi^2}} z \\ \dot{y} = x + y - \frac{1}{\sqrt{1+\varphi^2}} z + \mu x y - x^2 \\ \dot{z} = -\frac{\epsilon\varphi}{\sqrt{1+\varphi^2}} x + \frac{\epsilon}{\sqrt{1+\varphi^2}} y + (1-\varphi) z \end{cases} \tag{5.9}$$

The homoclinic orbit and its destruction as μ is varied around μ_0 can be visualized computing the orbit of a point P in the local unstable manifold of the origin. Since the flow of the system (5.9) behaves as the associated linear system in a neighbourhood of the origin, this starting point can be taken sufficiently close to the origin in the direction of the eigenvector $e_{\lambda_1} = (1, \varphi, 0)^T$ of eigenvalue λ_1. Notice that e_{λ_1} is independent of ϵ, hence the starting point of our orbit can be the same for different values of ϵ in (5.9). We take $P = (0,0,0) + 10^{-3} e_{\lambda_1} / \|e_{\lambda_1}\|_2$. The positive orbit of this point P for fixed values of μ and ϵ is computed using the Taylor integration method explained in Appendix B.

Fixed a value $\epsilon \geq 0$, the search of a value $\mu_0 \in \mathbb{R}$ for which the system (5.9) has a homoclinic orbit to the origin is done by looking for μ such that the orbit of P approximately returns to the origin. Here we considered the values $\epsilon_0 = 0$ and $\epsilon_1 = 1$ that have a homoclinic orbit to the origin when the parameter μ is $\mu_0 \approx -1.1534765$ and $\mu_1 \approx -0.600242325$ respectively.

For $\epsilon = \epsilon_0 = 0$ the origin is a saddle-node equilibrium of the system $X_{\mu_0,0,1}$. Therefore, it does not present a Shilnikov bifurcation with critical value μ_0, but a homoclinic orbit that resembles the Figure 1.1 in dimension 3, showing different values of the split function $\rho(\mu)$ in dimension 3. The first picture in Figure 5.2 shows that $\rho(\mu) < 0$ for $\mu > \mu_0$; the second picture illustrates the homoclinic orbit for $\mu = \mu_0$, i.e. $\rho(\mu_0) = 0$; and the third picture shows that $\rho(\mu) > 0$ for $\mu < \mu_0$.

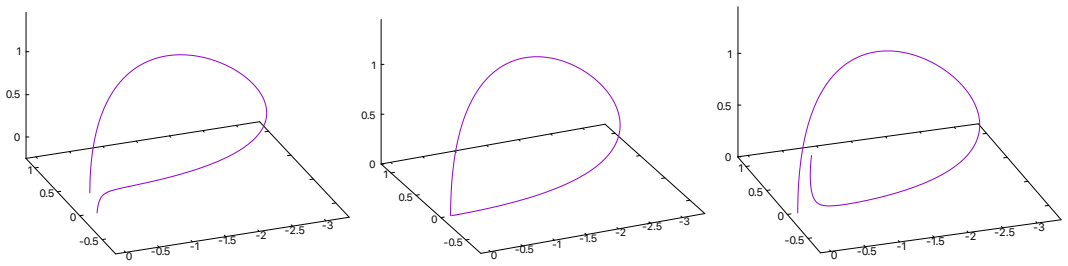

Figure 5.2: Homoclinic orbit of $X_{\mu,\epsilon_0,1}$ being destroyed as μ is varied around μ_0. See the text for details.

The system $X_{\mu,\epsilon_1,1}$ exhibits a Shilnikov bifurcation as μ is varied around μ_1. Figure 5.3 illustrates the homoclinic orbit of $X_{\mu_1,\epsilon_1,1}$ and its destruction as the parameter μ is varied around μ_1. These three pictures reveal some new details on the bifurcation. First, notice that in the second picture corresponding to the homoclinic orbit to the origin of the system $X_{\mu_1,\epsilon_1,1}$, we can slightly see that the homoclinic orbit spirals around the origin in the plane $z = 0$ as the orbit gets close to the origin, showing that it is in fact a saddle-focus equilibrium.

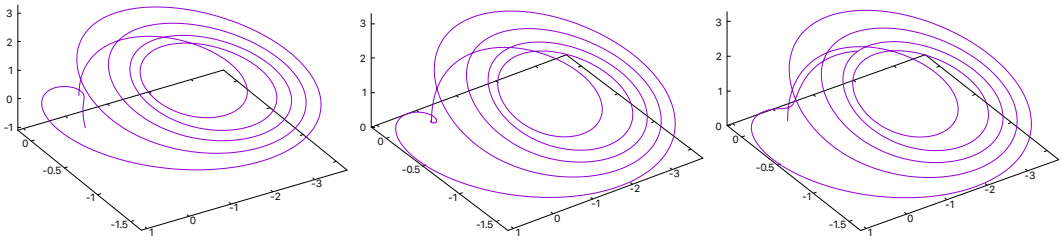

Figure 5.3: Homoclinic orbit of $X_{\mu,\epsilon_1,1}$ being destroyed as μ is varied around μ_1.

Additionally, it is clear that the number of loops that the homoclinic orbit does inside the image of the global diffeomorphism ψ_2 has increased with respect to the system $X_{\mu_0,\epsilon_0,1}$. The appearance of those loops does not contradict any previous statement because preserving the notation from Chapter 2, those loops lay in the image of the global diffeomorphism ψ_2 of which we have no control. Visually, one can define a cylinder C_+ around the origin, such that the loops do not intersect C_+ and the flux is linear in this cylinder. This is visualized in figure 5.4 using $\mu = -1.00857183$ and $\epsilon = 0.1$.

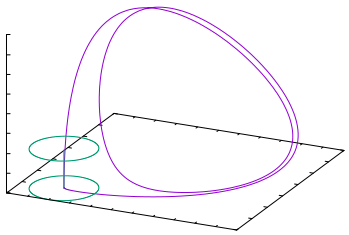

Figure 5.4: We illustrate that C_+ can be defined in a small neighbourhood of the origin that does not intersect the loops of the homoclinic orbit that lay in the image of the global diffeomorphism ψ_2.

By continuity, this reinforces the idea that there exist more than one curve in the plane of parameters (ϵ, μ) such that for all points (ϵ_H, μ_H) in this curve, the system $X_{\mu_H,\epsilon_H,1}$ has a homoclinic orbit to the origin. However, as we explained in section

5.1, this is just a conjecture, and little is known about these curves determining systems with homoclinic orbits.

5.3 Numerical study of the case $\sigma < 0$

In section 2.2 we saw that when $\sigma < 0$, there exist a unique stable limit cycle Γ_1 in a tubular neighbourhood of the homoclinic orbit Γ_0. However, it was not possible to study the exact type of stability of Γ_1 in the general case. In this section we will use the system (5.8) with $\delta = -1$, to illustrate orbits in a tubular neighbourhood of Γ_0 and see how they approach Γ_1. Furthermore, we will use a Poincaré section transversal to Γ_1 to determine its exact type of stability.

5.3.1 Illustration of the limit cycle

The system $X_{\mu,\epsilon,-1}(x,y,z)$ can be expressed as

$$X_{\mu,\epsilon,-1}(x,y,z): \begin{cases} \dot{x} = y + (\varphi - 1)z \\ \dot{y} = x - y - z + \mu xy - x^2 \\ \dot{z} = \epsilon(1-\varphi)x + \epsilon y - \varphi z \end{cases} \tag{5.10}$$

One can compute that the eigenvector of eigenvalue λ_{-1} of the matrix $DX_{\mu,\epsilon,-1}(0)$ is $e_{\lambda_{-1}} = (1, \varphi - 1, 0)^T$. Following a reasoning similar to the one used in section 5.2, take a point $P = (0,0,0) + 10^{-3} e_{\lambda_{-1}} / \|e_{\lambda_{-1}}\|_2$ that lays near the local unstable manifold of the origin. Since the coordinates of P do not depend on ϵ, this point can be used as a starting point for the Taylor method explained in Appendix B applied to the systems $X_{\mu,\epsilon,-1}, \forall \epsilon \in \mathbb{R}$. In Figure 5.5 we illustrate in purple the positive orbit of P tending to the limit cycle Γ_1 when $\mu = 1.025$ and $\epsilon = 0.1$.

Recall that in section 2.2, the limit cycle Γ_1 was seen as a fixed point p_0 of a $2-$dimensional Poincaré map $\mathcal{P}$. In order to visualize the type of stability of Γ_1, we shall consider as our Poincaré section a plane Π transversal to Γ_1 containing p_0, such that Π has $e_{\lambda_{-1}}$ as normal vector, i.e. points $(x,y,z) \in \Pi$ satisfy that $g(x,y,z) = 0$, where $g(x,y,z) = x + (\varphi - 1)y + D$ for an appropriate $D \in \mathbb{R}$.

The current aim is to compute points on $Or(P) \cap \Pi$. To this end, we compute points from $Or(P)$ with the Taylor method until we find two consecutive points $p(t_k) \in Or(P)$ and $p(t_{k+1}) = p(t_k + h) \in Or(P)$ such that $g(p(t_k)) < 0$ and $g(p(t_{k+1})) > 0$. Then, applying the bisection method, we find a suitable time step $h_* \in (0,h)$ which satisfies that $|g(p(t_k + h_*))| < tol$, for a sufficiently small $tol > 0$. In Figure 5.5 we illustrate the results for the system $X_{1.025,0.1,-1}$ with $D = -1$.

Additionally, in the right plot we isolate Γ_1 from the rest of the orbit of P. One can see that p_0 is a stable node, but this is just a visualization. In the next section we perform some checks on the stability of a stable limit cycle and explore the space of parameters (ϵ, μ) to find such cycles.

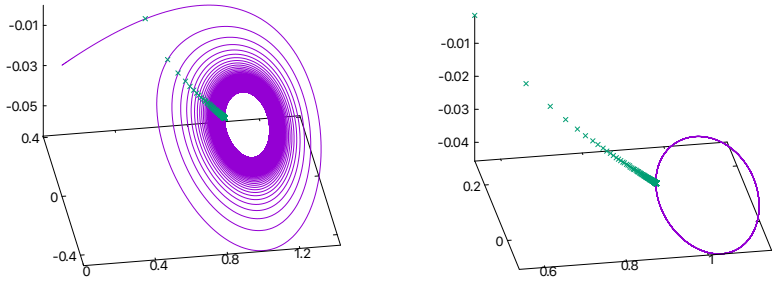

Figure 5.5: In the left plot we illustrate the positive orbit of P in purple and its intersection with Π taking $D = -1$ in green. The right one shows the limit cycle Γ_1 in purple and some points of the set $Or(P) \cap \Pi$.

5.3.2 On the set of parameters having a limit cycle and its stability

In section 2.2 we proved the existence of a stable limit cycle Γ_1 when $\rho(\gamma) > 0$ is sufficiently small. Therefore, we do not expect that the system $X_{\mu,\epsilon,-1}$ has a stable limit cycle Γ_1 for all values of μ and ϵ. Consequently, the first objective is to find values of μ and ϵ for which Γ_1 exists. To do that, we implement the following auxiliary algorithm. We take a uniform grid made of points $(\epsilon, \mu) \in [0, 2]^2$. For each of those points, consider the system $X_{\mu,\epsilon,-1}$ and apply the Taylor method starting at P taking a large maximum time so that the last point obtained $p_0 \in Or(P)$ is assumed to be close enough to Γ_1 in the case that it exists.

- **Case 1:** If $||X_{\mu,\epsilon,-1}(p_0)||_2 < tol$ for a fixed small value $tol > 0$, then p_0 is a fixed point, which in this case can be seen as a degenerated limit cycle.
- **Case 2:** If $||p_0||_2 > K$ for a relatively large and positive constant $K \in \mathbb{R}$, then the orbits of points in a tubular neighbourhood of the unstable manifold of the origin escape from that region, implying that Γ_1 does not exist.
- **Case 3:** Define a plane Π with normal vector $X_{\mu,\epsilon,-1}(p_0)$ and $p_0 \in \Pi$. Let $\mathcal{P} : \Pi \to \Pi$ be a Poincaré map, and compute $\mathcal{P}^n$ for a few values of $n \in \mathbb{N}$. If $||\mathcal{P}^{n_0}(p_0) - p_0||_2 < tol$ for a certain value $n_0 \in \mathbb{N}$, then Γ_1 exists.
- **Case 4:** If the Taylor methods arrives at the maximum time but Γ_1 exists, then either its stability is too slow, or it has an extremely large period.

We are only interested in Case 3 because Case 1 is degenerated, Case 2 does not present a limit cycle, and Case 4 is too hard to handle numerically. In Figure 5.6 we show the results on a 240×240 grid. Case 1 is represented in green, Case 2 in purple, Case 3 in blue and Case 4 in yellow.

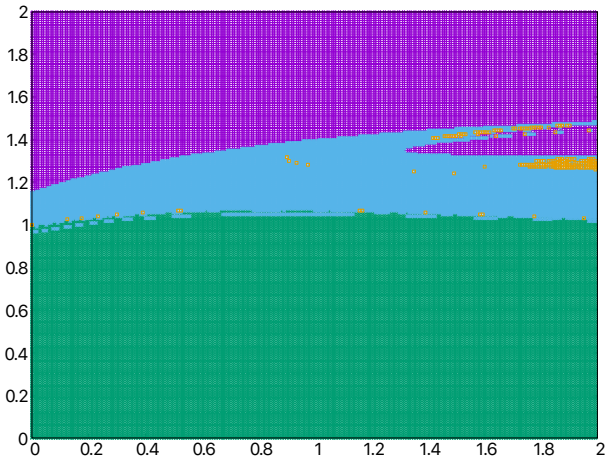

Figure 5.6: Different assimptotic behaviours of system $X_{\mu,\epsilon,-1}$ as a function of (ϵ, μ).

Notice that Figure 5.6 gives much more valuable information than the location of limit cycles in the parameters space (ϵ, μ). One sees that for some values of $\epsilon \geq 1.4$, there exist at least two disjoint intervals containing values of μ, in which $X_{\mu,\epsilon,-1}$ has a stable limit cycle. As we saw in section 2.2, the stable limit cycle accumulates into the homoclinic orbit when the split function tends to zero. Therefore, this numerical experiment reinforces the idea that there exists more than one curve γ_H in the space of parameters (ϵ, μ) such that $\forall(\epsilon, \mu) \in \gamma_H$, the system $X_{\mu,\epsilon,-1}$ has a homoclinic orbit to the origin. Additionally, it is reasonable to expect that systems containing homoclinic orbits have parameters laying in one of the boundaries separating a purple and a blue region. In Figure 5.7 we zoom into interesting regions and generate a bigger grid of points for a better visualiation.

In the left plot of Figure 5.7 we see that the transition from the green region to the blue one is not given by the crossing throughout a curve as one would expect from Figure 5.6. In particular, one can see that the blue region is the union of at least two disjoint connected components inside the compact $[0, 2]^2$. From this, we deduce that fixing a value $\epsilon_0 \in [0, 2]$, then the one-parametric system $X_{\mu,\epsilon_0,-1}$ may exhibit some bifurcations as the parameter μ is varied. Let Γ_1 be a stable limit cycle emerging at a system with parameters laying in the blue region. Moreover

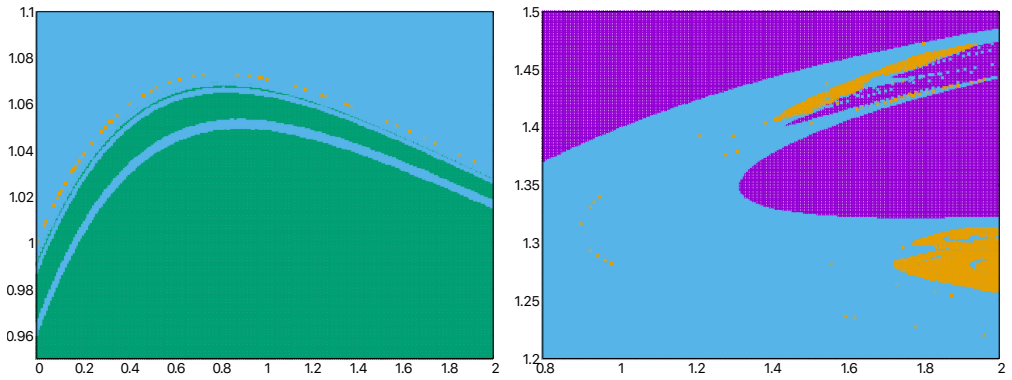

Figure 5.7: Zooms in regions of interest from Figure 5.6 taking a larger grid of points for a better visualization.

we have checked that the number of turns of Γ_1 before closing is widely varied, which is consistent with the fact that the blue region is not a unique connected component.

In the right plot of Figure 5.7 we see that there are a few yellow regions in the compact $[0,2]^2$. As we already mentioned, the periods of the limit cycles in the blue regions vary a lot. Therefore, it is very likely that those yellow regions correspond to systems having a stable limit cycle with a really large period.

Remark 5.2. We empathize that the previous observations are based on preliminary numerical experiments. A full understanding of the scenarios escapes from the aims and aspirations of this project.

After discussing the rich dynamics exhibited in the systems $X_{\mu,\epsilon,-1}$, we can now analize the stability of a given limit cycle. Consider (ϵ,μ)in the blue region of Figure 5.6 and a point $p_0 \in \Gamma_1$. Define a plane Π with normal vector $X_{\mu,\epsilon,-1}(p_0)$ and such that $p_0 \in \Pi$. Consider the Poincaré map $\mathcal{P} : \Pi \to \Pi$. Then, p_0 is a stable node if the eigenvalues of $D\mathcal{P}(p_0)$ are real, and p_0 is a stable focus if the eigenvalues of $D\mathcal{P}(p_0)$ are complex and conjugated. We approximate $D\mathcal{P}$ by taking a basis $\{u_1, u_2\}$ of $T_{p_0}\Pi$ and using the centered numerical differentiation formula with a suitable small step h. Then, we check the sign of $(tr(D\mathcal{P}(p_0)))^2 - 4Det(D\mathcal{P}(p_0))$ to decide if the eigenvalues are real or not. Our computations show that all the cases considered correspond to stable node cycles. However, a limit cycle of focus type could exist for other values of the parameters, but further numerical experiments are needed to clarify this.

Conclusions

In this work, we studied the rich dynamics of $3-$dimensional continuous parametric systems containing a homoclinic orbit to a saddle-focus equilibrium. To do that, we reduced the original system into a discrete $2-$dimensional one using Poincaré sections. Moreover, we studied the horseshoe map using symbolic dynamics to understand its chaotic behaviour and its relation with other systems. All of that made it possible to prove the Shilnikov Theorem, which describes the most complicated dynamics presented in a system exhibiting a Shilnikov bifurcation. Furthermore, we used those theoretical results to make numerical simulations and illustrate some scenarios and properties involving this bifurcation.

Several related topics might be of interest for future studies. Some of them have been briefly mentioned in this project or are natural next step extensions of the presented results. For example:

- Study the case $\sigma = 0$ first discussed in [Bel84]. The conservative case is included in this setting; hence, it would be interesting to understand the transition as the saddle value is varied across $\sigma = 0$.
- In Chapter 5 we appealed to perturbation theory to assume that homoclinic orbits to the origin exist for small values of ϵ. We could compute the invariant manifolds and check that they intersect for large values of ϵ, see [GL96]. The role of the $1-$dimensional and $2-$dimensional invariant manifolds in the bifurcation scenario is discussed in [AKO14].
- Study the discrete analogous of the Shilnikov bifurcation. Note that results from the discrete case cannot be deduced directly from the continuous one.
- Consider homoclinic bifurcations in higher dimensions motivated by the rich dynamics exhibited in 3-dimensional systems. A study of the focus-focus homoclinic bifurcation in dimension four is discussed in [Kuz13]. The techniques we showed in Section 5.1 could also be used to obtain explicit systems in higher dimensions with the desired properties.

Appendices

Appendix A

Technical proofs

Some of the proofs in this work are pretty technical and make substantial use of other branches in Mathematics, whose deep understanding is not the main purpose of this project. However, an insight into these was required to complete more complex proofs or gain some further knowledge in the context in which they appear. Therefore, we provide in this Appendix the proof of all those results which are just stated in the main work and whose proof is considered significant for the completion of this project.

A.1 Proposition 1.16

Suppose that the system $\dot{x} = f(x)$ has a homoclinic orbit Γ_0 to a hyperbolic equilibrium $x_0 \in \mathbb{R}^n$. Let $n_+, n_-, W^u(x_0)$ and $W^s(x_0)$ be the amount of positive and negative eigenvalues of $Df(x_0)$, and the unstable and stable sets of x_0 respectively. Since Γ_0 is a homoclinic orbit to x_0, we know that $n_+ > 0, n_- > 0, n_+ + n_- = n$ and $\Gamma_0 \subseteq W^u(x_0) \cap W^s(x_0)$.
We know that $\forall x \in \Gamma_0$, $T_x W^u(x_0)$ and $T_x W^s(x_0)$ are generated by n_+ and n_- linearly independent vectors respectively. Moreover, $f(x)$ is tangent to both $W^u(x_0)$ and $W^s(x_0)$, hence the maximum amount of independent vectors tangent to $W^u(x_0)$ and $W^s(x_0)$ at $x \in W^u(x_0) \cap W^s(x_0)$ is: $n_+ + n_- - 1 = n - 1 < n$, which indicates that $W^u(x_0)$ and $W^s(x_0)$ are not transverse.
If a perturbation breaks the homoclinic orbit Γ_0, then this new perturbed system will not be topologically equivalent to the original one in a region around Γ_0, implying that Γ_0 is structurally unstable. Otherwise, if the homoclinic orbit is preserved by some perturbation, we just proved that the stable and unstable manifolds of the saddle-focus of the perturbed system are transverse, which contradicts the fact that transversality is a generic property. Hence this case can not occur under the effect of generic perturbations.

A.2 Theorem 2.4 (Banach Fixed Point Theorem)

Take $x_0 \in X$ and consider the sequence $(x_n)_{n\geq 0}$. For all $n \geq 0$ we have the following inequality:

$$d(x_{n+1}, x_n) = d(f(x_n), f(x_{n-1})) \leq k\, d(x_n, x_{n-1})$$

Inductively we deduce that $d(x_{n+1}, x_n) \leq k^n\, d(x_1, x_0)$. Using that and the triangle inequality, $\forall n, m \in \mathbb{N}$ with $n > m$, it is satisfied that:

$$d(x_n, x_m) \leq \sum_{i=m}^{n-1} d(x_{i+1}, x_i) \leq k^m\, d(x_1, x_0) \sum_{i=0}^{n-m-1} k^i = k^m\, d(x_1, x_0) \frac{1}{1-k}$$

Since $k \in (0,1)$, then $\forall \epsilon > 0, \exists N \in \mathbb{N}$ large enough such that $k^N < \epsilon \frac{1-k}{d(x_1,x_0)}$. Choosing $N < m < n$ we have that:

$$d(x_n, x_m) \leq k^m\, d(x_1, x_0) \frac{1}{1-k} < \epsilon \cdot \frac{1-k}{1-k} \cdot \frac{d(x_1, x_0)}{d(x_1, x_0)} = \epsilon$$

Therefore, $(x_n)_{n\geq 0}$ is a Cauchy sequence, and because of X being complete, $(x_n)_{n\geq 0}$ is also convergent, which means that there exist a point $p \in X$ such that $p = \lim_{n\to\infty} x_n$. This point p is fixed by f:

$$p = \lim_{n\to\infty} x_n = \lim_{n\to\infty} f(x_{n-1}) = f(\lim_{n\to\infty} x_{n-1}) = f(p)$$

Uniqueness is proven by contradiction. Take $p, q \in X$ with $f(p) = p, f(q) = q$ and $p \neq q$, then:

$$d(p, q) = d(f(p), f(q)) \leq k\, d(p, q)$$

That is not possible because $k \in (0,1)$, hence $p = q$.

A.3 Lemma 3.9

For each vertical strip V_k there exist two vertical curves $v_k^1(y), v_k^2(y)$ such that $V_k = \{(x, y) : x \in [v_k^1, v_k^2], \forall y \in [0,1]\}$. In addition we have the following:

$$\begin{aligned} \lim_{k\to\infty} d(V_k) = 0 &\iff \lim_{k\to\infty} (\max_{y\in[0,1]} |v_k^2(y) - v_k^1(y)|) = 0 \iff \\ &\iff \lim_{k\to\infty} |v_k^2(y) - v_k^1(y)| = 0, \forall y \in [0,1] \end{aligned}$$

Therefore $\bigcap_{k=1}^{\infty} V_k$ is the vertical curve $\lim_{k\to\infty} v_k^1(y) = \lim_{k\to\infty} v_k^2(y)$ for $y \in [0,1]$.

A.4 Lemma 3.11

A point (x_0, y_0) lays in the intersection of $x = v(y)$ and $y = h(x)$ if and only if $x_0 = v(y_0) = v(h(x_0))$. Therefore we want to find the zeroes of the function $g(x) = x - v(h(x))$. By definition 3.7, if $0 \leq x_1 \leq x_2 \leq 1$, then:

$$|v(h(x_2)) - v(h(x_1))| \leq \mu \cdot |h(x_2) - h(x_1)| \leq \mu^2 |x_2 - x_1|$$

Since $\mu^2 \in (0, 1)$, the function $g(x)$ is strictly monotonically increasing. Moreover:

$$g(0) = 0 - v(h(0)) \leq 0 \quad \text{and} \quad g(1) = 1 - v(h(1)) \geq 0$$

because $v, h : [0, 1] \to [0, 1]$. Consequently $g(x)$ has exactly one zero which is the point of intersection between the vertical curve $x = v(y)$ and the horizontal curve $y = h(x)$.

A.5 Lemma 3.12

Set the coordinates $p_1 = (x_1, y_1)$ and $p_2 = (x_2, y_2)$. Since $p_1 = h_1 \cap v_1$, it is satisfied that $x_1 = v_1(y_1)$ and similarly $x_2 = v_2(y_2)$. Therefore, using the triangle inequality, the definition of vertical curve and the norm over vertical curves, one has that:

$$|x_2 - x_1| \leq |v_2(y_2) - v_1(y_2)| + |v_1(y_2) - v_1(y_1)| \leq ||v_2 - v_1|| + \mu |y_2 - y_1|$$

Analogously, since $y_1 = h_1(x_1)$ and $y_2 = h_2(x_2)$, applying the definitions for horizontal curves, one has that:

$$|y_2 - y_1| \leq |h_2(x_2) - h_1(x_2)| + |h_1(x_2) - h_1(x_1)| \leq ||h_2 - h_1|| + \mu |x_2 - x_1|$$

In consequence:

$$\begin{aligned} |p_2 - p_1| &= |x_2 - x_1| + |y_2 - y_1| \leq \\ &\leq \mu(|x_2 - x_1| + |y_2 - y_1|) + ||h_2 - h_1|| + ||v_2 - v_1|| = \\ &= \mu |p_2 - p_1| + ||h_2 - h_1|| + ||v_2 - v_1|| \end{aligned}$$

Therefore, taking the extremes of the inequalities, we can conclude that:

$$|p_2 - p_1| \leq \frac{1}{1 - \mu}(||h_2 - h_1|| + ||v_2 - v_1||)$$

A.6 Proposition 3.14

Let H_i and H_j be horizontal strips with $i, j \in I_N$ such that $\gamma \subset H_j$ is a horizontal curve and by $\mathcal{H}1$, $H_i = f^{-1}(V_i)$ for a certain vertical strip V_i, see Figure A.1. By lemma 3.11, γ intersects each vertical boundary of V_i in precisely one point and $\overline{\gamma} = \gamma \cap V_i$ is a curve joining them. From $\mathcal{H}1$ one deduces that $f^{-1}(\overline{\gamma})$ is a curve joining the vertical boundaries of H_i that lay in $x = 0$ and $x = 1$.

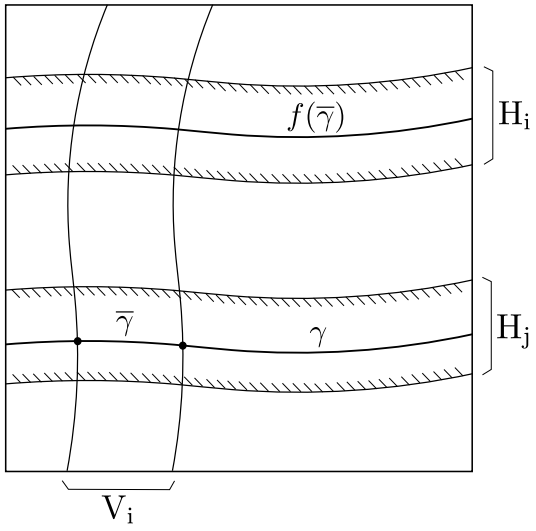

Figure A.1: Strips and curves involved in the proof of Prop 3.14.

We want to prove that $f^{-1}(\overline{\gamma}) = f^{-1}(\gamma) \cap H_i$ is a horizontal curve. Since γ is a horizontal curve, by definition 3.7, it can be expressed as $y = h(x)$ with:

$$|h(x_1) - h(x_2)| \leq \mu |x_1 - x_2| \quad , \quad 0 \leq x_1 < x_2 \leq 1$$

Recalling that $Df^{-1}(S^s) \subset S^s$, one has as a consequence of the mean value theorem that if $(x_1, y_1), (x_2, y_2) \in f^{-1}(\overline{\gamma})$, then $|y_1 - y_2| \leq \mu |x_1 - x_2|$. In other words, $f^{-1}(\overline{\gamma})$ is a curve of the form $y = \overline{h}(x)$ such that $|\overline{h}(x_1) - \overline{h}(x_2)| \leq \mu |x_1 - x_2|$, which is the definition of $f^{-1}(\overline{\gamma})$ being a horizontal curve.

Applying twice what we just proved with γ being the horizontal boundaries of a horizontal strip $H \subset H_j$, it is concluded that $f^{-1}(H)$ is a horizontal strip. In particular, $\overline{H_i}$ defined as $\overline{H_i} = f^{-1}(H) \cap H_i = f^{-1}(H \cap V_i)$ is a horizontal strip as we wanted to prove. The proof for vertical strips is similar and can be found in [Mos01].

It remains to prove that $\mathcal{H}2$ holds with $0 < \mu < \frac{1}{2}$ and $\nu = \frac{\mu}{1-\mu}$. Take two points $p_1 = (x_1, y_1), p_2 = (x_2, y_2)$ from the horizontal boundaries of $\overline{H_i}$ such that $x_1 = x_2$ and $d(\overline{H_i}) = |p_1 - p_2|$. Then, $s(t) = (1-t)p_1 + tp_2$ is a vertical segment joining p_1 and p_2, hence $s'(t) \in S^u$. By $\mathcal{H}3$, if $z(t) = f(s(t))$, then $z'(t) \in S^u$. In particular, one can build a vertical curve $\overline{z}(t)$ extending $z(t)$ with vertical segments, and by construction, $z(0), z(1) \in \overline{z}(t)$. Additionally, since $\overline{H_i} = f^{-1}(H \cap V_i), d(\overline{H_i}) = |p_1 - p_2|$ and $z(t) = f(s(t))$, there must exist two horizontal curves h_1 and h_2 such that $z(0) = h_1 \cap \overline{z}(t)$, $z(1) = h_2 \cap \overline{z}(t)$ and the distance between h_1 and h_2 is $d(H \cap V_i)$.

If $z(t) = (x(t), y(t))$, applying the fundamental theorem of calculus, the inequalities given by $\mathcal{H}3$ and lemma 3.12 with $v_1 = v_2 = \overline{z}$, one has:

$$\begin{aligned} |p_1 - p_2| = \int_0^1 |s'(t)|dt \leq \mu \int_0^1 |y'(t)|dt = \mu|y(1) - y(0)| \leq \\ \leq \mu(|y(1) - y(0)| + |x(1) - x(0)|) = \mu|z(1) - z(0)| \leq \\ \leq \frac{\mu}{1-\mu} d(H \cap V_i) \end{aligned}$$

Then, it can be concluded that:

$$d(f^{-1}(H \cap V_i)) = d(\overline{H_i}) = |p_1 - p_2| \leq \nu d(H \cap V_i) \text{ with } \nu = \frac{\mu}{1-\mu}.$$

A.7 Theorem 3.15

First of all, we will find a map h meeting the desired properties. Define inductively the vertical strips $V_{s_{-1}s_{-2}\ldots s_{-n}} = f(V_{s_{-2}s_{-3}\ldots s_{-n}}) \cap V_{s_{-1}}$ and the horizontal strips $H_{s_0 s_1 \ldots s_n} = f^{-1}(H_{s_1 \ldots s_n}) \cap H_{s_0}$, where $s_k \in I_N, \forall k \in \mathbb{Z}$. Hypothesis $\mathcal{H}2$ gives the following inequalities:

$$d(V_{s_{-1}s_{-2}\ldots s_{-n}}) \leq \nu d(V_{s_{-2}\ldots s_{-n}}) \leq \ldots \leq \nu^{n-1} d(V_{s_{-n}}) \leq \nu^{n-1}$$

$$d(H_{s_0 s_1 \ldots s_n}) \leq \nu d(H_{s_1 \ldots s_n}) \leq \ldots \leq \nu^n d(H_{s_n}) \leq \nu^n$$

Taking the limit as $n \to \infty$, $\nu^{n-1} \to 0$ and $\nu^n \to 0$ because $\nu \in (0, 1)$. Additionally, $V_{s_{-1}s_{-2}\ldots s_{-n}} \subset V_{s_{-2}\ldots s_{-n}} \subset V_{s_{-n}}$ and $H_{s_0 s_1 \ldots s_n} \subset H_{s_1 \ldots s_n} \subset H_{s_n}$ are sequences of vertical and horizontal strips respectively. Therefore, by lemma 3.9 there exist a vertical curve $V(s)$ and a horizontal curve $H(s)$ such that:

$$V(s) = \bigcap_{n=1}^{\infty} V_{s_{-1}s_{-2}\ldots s_{-n}} \quad \text{and} \quad H(s) = \bigcap_{n=0}^{\infty} H_{s_0 s_1 \ldots s_n}$$

By lemma 3.11, $V(s)$ and $H(s)$ intersect in exactly one point $p = V(s) \cap H(s)$. We can associate to p the sequence $s(p) = \{\ldots s_{-n} \ldots s_{-2} s_{-1} \cdot s_0 s_1 \ldots s_n \ldots\} \in \Sigma$.

Now, one wants to find the sequence associated to $f(p)$. To do that, we will compute $f(p) = f(V(s)) \cap f(H(s))$. The following equivalences are deduced from the definitions and the fact that f is a homeomorphism:

$$H_{s_0 s_1 \dots s_n} = f^{-1}(H_{s_1} \dots s_n) \cap H_{s_0} \implies f(H_{s_0 s_1 \dots s_n}) = H_{s_1 \dots s_n} \cap f(H_{s_0})$$

By $\mathcal{H}1$ it is known that $f(H_{s_0}) = V_{s_0}$, therefore:

$$f(H_{s_0 s_1 \dots s_n}) = H_{s_1 \dots s_n} \cap V_{s_0}$$

Using that last equality and the definition $V_{s_0 s_{-1} \dots s_{-n}} = f(V_{s_{-1}} \dots s_{-n}) \cap V_{s_0}$ we can finally compute $f(p)$:

$$\begin{aligned} f(p) &= \left(\bigcap_{n=1}^{\infty} f(V_{s_{-1} s_{-2} \dots s_{-n}}) \right) \cap \left(\bigcap_{n=0}^{\infty} f(H_{s_0 s_1 \dots s_n}) \right) = \\ &= \left(\bigcap_{n=1}^{\infty} f(V_{s_{-1} s_{-2} \dots s_{-n}}) \right) \cap \left(\bigcap_{n=1}^{\infty} H_{s_1 \dots s_n} \cap V_{s_0} \right) = \\ &= \left(\bigcap_{n=1}^{\infty} f(V_{s_{-1} s_{-2} \dots s_{-n}}) \cap V_{s_0} \right) \cap \left(\bigcap_{n=1}^{\infty} H_{s_1 \dots s_n} \right) = \\ &= \left(\bigcap_{n=0}^{\infty} V_{s_0 s_{-1} \dots s_{-n}} \right) \cap \left(\bigcap_{n=1}^{\infty} H_{s_1 \dots s_n} \right) \end{aligned}$$

Consequently, the sequence associated to $f(p)$ is:

$$\sigma(s(p)) = \{ \dots s_{-n} \dots s_{-2} s_{-1} s_0 \cdot s_1 \dots s_n \dots \}$$

where σ is the shift map. Therefore, it is clear that $h : \Sigma \to \Lambda$ defined as $h(s(x)) = x$ for $x \in \Lambda$ mapping sequences into points as shown, satisfies that $f_{\restriction \Lambda} \circ h = h \circ \sigma$. Moreover Λ is the compact invariant set defined by:

$$\Lambda = \bigcap_{k \in \mathbb{Z}} f^k \left(\bigcup_{i \in I_N} V_i \right)$$

To prove that h is continuous, we will use the distance between sequences from lemma 3.1. Take two sequences $s, s' \in \Sigma$ such that $s_k = s'_k, \forall |k| \leq j$ for a certain $j \in \mathbb{N}$. Then by construction, the points $p = h(s)$ and $p' = h(s')$ lay in $V_{s_{-1} \dots s_{-j}} \cap H_{s_0 \dots s_j}$. By $\mathcal{H}2$ one knows that $d(V_{s_{-1} \dots s_{-j}}) < \nu^{j-1}$ and $d(H_{s_0 \dots s_j}) < \nu^j$ for a certain $\nu \in (0, 1)$. Therefore $V_{s_{-1} \dots s_{-j}} \cap H_{s_0 \dots s_j}$ is a region bounded by two vertical curves with a maximum distance of ν^{j-1}, and two horizontal curves with maximum distance of ν^j. Thus, lemma 3.12 bounds the maximum distance between two points in this region:

$$|p - p'| \leq \frac{1}{1 - \mu} \left(\nu^{j-1} + \nu^j \right)$$

which tends to 0 as j tends to infinity. In conclusion, $\forall \epsilon > 0$ if we choose $j \in \mathbb{N}$ large enough, $\exists \delta > 0$ such that $d(s, s') < \delta \implies |p - p'| < \epsilon$. Since p and p' were arbitrary, we deduce that h is continuous.
By $\mathcal{H}1$, the horizontal and vertical strips H_i and V_i are disjoint for every $i \in I_N$, therefore h is injective. Moreover, h is exhaustive because every point $p \in \Lambda$ lays in the intersection of vertical and horizontal strips. Hence we can construct a sequence $s(p)$ as specified before.

Since I_N is assumed to be finite in $\mathcal{H}1$, and h is continuous and injective, one concludes that h^{-1} is continuous and hence h is a homeomorphism. It remains to prove the hyperbolicity of Λ under the assumptions of the Theorem.

Take a point $p \in \Lambda$ and denote:

$$Df^{-1}(p) = \begin{pmatrix} a & b \\ c & d \end{pmatrix}$$

By $\mathcal{H}3$, p has associated the cone $S^s = \{(\xi, \eta) : |\eta| < \mu|\eta|\}$. Consider two linearly independent lines L_p^+ and L_p^- laying in S^s and intersecting in p. Since $L_p^+, L_p^- \subset S^s$, they must vary continuously with p and $Df^{-1}(L_p^{\pm}) = L_{f^{-1}(p)}^{\pm}$. Moreover, they can be expressed as:

$$\eta = \alpha_p \xi, \text{ with } |\alpha_p| \leq \mu$$

where α_p is a continuous function on p. Applying Df^{-1} to that expression, one gets:

$$\begin{pmatrix} \xi_1 \\ \eta_1 \end{pmatrix} = \begin{pmatrix} a & b \\ c & d \end{pmatrix} \begin{pmatrix} \xi \\ \eta \end{pmatrix} \iff \begin{pmatrix} \xi_1 \\ \eta_1 \end{pmatrix} = \begin{pmatrix} a\xi + b\eta \\ c\xi + d\eta \end{pmatrix} \tag{A.1}$$

Taking the quotient between the two coordinates and recalling that $\eta = \alpha_p \xi$, we get the relation between η_1 and ξ_1:

$$\frac{\xi_1}{\eta_1} = \frac{a\xi + b\eta}{c\xi + d\eta} \iff \eta_1 = \frac{c\xi + d\eta}{a\xi + b\eta}\xi_1 = \frac{c + d\alpha_p}{a + b\alpha_p}\xi_1$$

If $\alpha^*_{f^{-1}(p)} = \frac{c+d\alpha_p}{a+b\alpha_p}$, that is equivalent to $\eta_1 = \alpha^*_{f^{-1}(p)}\xi_1$. By $\mathcal{H}3$ we know that $|\xi_1| \geq \frac{1}{\mu}|\xi|$. Comparing this inequality with the first coordinate of equation (A.1), we obtain the following inequality:

$$|\xi_1| = |a\xi + b\eta| = |\xi| \cdot |(a + b\alpha_p)| \implies |a + b\alpha_p| \geq \frac{1}{\mu}$$

Consider another pair of lines in S^s given by $\eta = \beta_p \xi$ with $|\beta_p| \leq \mu$ having the same properties as the first pair of lines. Using the equalities we just saw and the

last hypothesis of the Theorem, one can bound the distance between $\alpha^*_{f^{-1}(p)}$ and $\beta^*_{f^{-1}(p)}$:

$$\begin{aligned}\left|\frac{c+d\alpha_p}{a+b\alpha} - \frac{c+d\beta_p}{a+b\beta_p}\right| &\leq \frac{|Det(Df^{-1}(p))|}{|a+b\alpha_p|\cdot|a+b\beta_p|}|\alpha_p-\beta_p| \leq \\ &\leq \mu^2|Det(Df^{-1}(p))|\cdot|\alpha_p-\beta_p| \leq \\ &\leq \frac{1}{2}|\alpha_p-\beta_p|\end{aligned}$$

Since Λ is invariant under f^{-1}, that last boundary does not depend on the supporting point, hence:

$$\sup_{p\in\Lambda}|\alpha^*_p-\beta^*_p| \leq \frac{1}{2}\sup_{p\in\Lambda}|\alpha_p-\beta_p| \tag{A.2}$$

We can define a function g with domain the space of pairs of lines with the properties of L^+_p and L^-_p in S^s such that $g(L)_p = (Df^{-1}L)_{f^{-1}(p)}$, where L is any of those pairs of lines. Then, inequality (A.2) grants that g is a contraction mapping, hence by Theorem 2.4 S^s has a unique pair of fixed lines by g. By $\mathcal{H}3$ with $0<\mu<\frac{1}{2}$, under iteration by g these lines tend to a single stable invariant line, whose direction generates the vector space E^s_p.

Repeating the same procedure with lines defined in S^u, one gets an invariant line generating the vector space E^u_p, which is independent to E^s_p because S^s and S^u are disjoint by $\mathcal{H}3$. Therefore, since $p\in\Lambda$ was an arbitrary point, we can conclude that $T_\Lambda\mathbb{R}^2 = E^s_\Lambda \oplus E^u_\Lambda$.

Moreover, the inequalities $|\eta_1| \geq \frac{1}{\mu}|\eta_0|$ and $|\xi_{-1}| \geq \frac{1}{\mu}|\xi_0|$ from $\mathcal{H}3$ grant that taking $\lambda=\mu$ and $C=1$, the hyperbolicity conditions from definition 3.5 are satisfied. Consequently, Λ is a hyperbolic set.

Appendix B

Taylor method for the numerical integration of ODEs

B.1 Taylor Integration Method

The Taylor integration method is a numerical method to find points of a smooth function $x : [a, b] \to \mathbb{R}^n$ solving the Cauchy problem:

$$\begin{cases} \dot{x} = f(t, x) \\ x(a) = x_0 \end{cases}$$

where $f : [a, b] \times \mathbb{R}^n \to \mathbb{R}^n$ is a smooth function and $n \geq 1$. Here we will explain the method and apply it to the vector fields obtained in section 5.1. For further details, see [JZ05].

Let us denote $x_k = x(t_k)$ and assume that we start with a point $x_0 = x(a)$. The algorithm computes a point $x_{k+1} \in \mathbb{R}^n$ with $k \geq 0$ recursively from the previously computed points $x_0, ..., x_k$ using the Taylor series of $x_k = x(t_k)$ as follows:

$$x_{k+1} = x_k + x'(t_k)h + \frac{x''(t_k)}{2!}h^2 + \ldots + \frac{x^{(m)}(t_k)}{m!}h^m \tag{B.1}$$

There, $h \in \mathbb{R}$ is the time step defined by $t_{k+1} = t_k + h$, and $m \in \mathbb{N}$ is the order of the Taylor series. Here, we will fix the order at $m = 24$ and then compute an appropriate time step h_k for each point x_k of the orbit.

One can see that the Taylor method has the advantage of having full control on the precision of the points x_k because the order m can be increased as much as needed, whenever this does not lead to numerical issues. Moreover, the time

step h can be decreased to obtain more points of $x(t)$ in a fixed time interval if the function $x(t)$ requires it or if one wants a better visualization. The only problem with this method is that the derivatives of $x(t)$ are hard to compute in general, but this can be done using automatic differentiation.

Definition B.1. Let $f : I \subset \mathbb{R} \to \mathbb{R}$ be a smooth function. We define its normalized $n-$th derivative as:

$$f^{[n]}(t) = \frac{f^{(n)}(t)}{n!}$$

One can see that with this definition, equation (B.1) can be rewritten using the normalized derivatives of $x(t)$:

$$x_{k+1} = x_k + x^{[1]}(t_k)h + x^{[2]}(t_k)h^2 + \ldots + x^{[m]}(t_k)h^m \tag{B.2}$$

Therefore, for what concerns us, the problem of finding the derivatives of $x(t)$ is equivalent to the problem of finding the normalized derivatives of $x(t)$. This new equivalent goal is easier to accomplish because normalized derivatives have, among others, the following properties:

Proposition B.2. Let $g, h : I \subset \mathbb{R} \to \mathbb{R}^n$ be functions of class $\mathcal{C}^n$. Then, the following properties hold:

1. If $f(t) = g(t) \pm h(t)$, then $f^{[n]}(t) = g^{[n]}(t) \pm h^{[n]}(t)$.
2. If $f(t) = g(t)h(t)$, then $f^{[n]}(t) = \sum_{j=0}^{n} g^{[n-j]}(t)h^{[j]}(t)$.

Proof. The first property follows from the linearity of the derivatives:

$$f^{[n](t)} = (g(t) \pm h(t))^{[n]} = \frac{(g(t) \pm h(t))^{(n)}}{n!} = \frac{g^{(n)}(t)}{n!} \pm \frac{h^{(n)}(t)}{n!} = g^{[n]}(t) \pm h^{[n]}(t)$$

The second property is proven using the Leibniz's formula:

$$f^{[n]}(t) = \frac{1}{n!}f^{(n)}(t) = \frac{1}{n!}\sum_{j=0}^{n}\binom{n}{j}g^{(n-j)}(t)h^{(j)}(t) = \sum_{j=0}^{n} g^{[n-j]}(t)h^{[j]}(t)$$

□

This last proposition is helpful because now we can compute $x^{[k]}(t)$ decomposing it into simpler normalized derivatives.

B.2 Application to $X_{\mu,\epsilon,\delta}(x,y,z)$

In this section, we will explain the implementation of the Taylor method applied to the vector field $X_{\mu,\epsilon,1}$. To do that, we shall refer to the code from section B.3. Then, we will see that, with very few modifications to the code, we can obtain an implementation of the Taylor method applied to the vector field $X_{\mu,\epsilon,-1}$.

Consider the vector field $X_{\mu,\epsilon,1}(x,y,z)$ that describes the following system of differential equations seen in section 5.2:

$$X_{\mu,\epsilon,1}(x,y,z): \begin{cases} \dot{x} = y + \frac{\varphi}{\sqrt{1+\varphi^2}} z \\ \dot{y} = x + y - \frac{1}{\sqrt{1+\varphi^2}} z + \mu x y - x^2 \\ \dot{z} = -\frac{\epsilon\varphi}{\sqrt{1+\varphi^2}} x + \frac{\epsilon}{\sqrt{1+\varphi^2}} y + (1-\varphi) z \end{cases} \tag{B.3}$$

Before explaining the algorithm itself, let us explain the purpose of some of the variables involved in the main program. Variable *tmax* sets the maximum time that we will consider in our orbit. It is essential to choose the value of *tmax* carefully, because near homoclinic points, if small approximation errors place a point in a very unstable orbit and *tmax* is large, the orbit can get out of control and arrive at points really far away from the origin. The variables *hmax* and *hmin* are there to control that the step size is reasonable to draw enough points of the orbit without accumulating them. The vector *x* contains the coordinates of the last point of the orbit computed by the Taylor method. Since points are saved in a file, this value is updated each time the *taylor* function is called.

Now, let us explain some variables from the *taylor* function. Variable *diri* indicates the direction of time establishing if we are computing a positive or negative orbit of a point. The value of *diri* is determined depending on the initial time and the value of *tmax*. Variable $flag$ is the returning value of the *taylor* function, which is 1 if we arrived to *tmax* and 0 otherwise. Vectors $dx, dy, dz, dxp2$ and $dxdy$ store the values of some normalized derivatives that we will specify soon.

The main function simply calls the *taylor* function (lines 51-54) until one time step surpasses *tmax*, and prints all the points that we obtain in a file. The *taylor* function computes x_{k+1} using equation (B.2).

The normalized $n-$th derivative of the next point x_{k+1} is computed using Prop B.2 to decompose the vector field $X_{\mu,\epsilon,1}$, which tells us an expression for the next derivative, into simpler functions. In particular, the normalized derivatives are

computed up to order 24 (lines 119-140) using the following scheme for $n = 0, 1, 2, ..., 23$:

$$\begin{aligned}
u_1^{[n]}(t) &= x^{[n]}(t) \\
u_2^{[n]}(t) &= y^{[n]}(t) \\
u_3^{[n]}(t) &= z^{[n]}(t) \\
u_4^{[n]}(t) &= \sum_{j=0}^{n} u_1^{[n-j]}(t) u_1^{[j]}(t) \\
u_5^{[n]}(t) &= \sum_{j=0}^{n} u_1^{[n-j]}(t) u_2^{[j]}(t) \\
x^{[n+1]}(t) &= \frac{1}{n+1}\left(u_2^{[n]}(t) + \frac{\varphi}{\sqrt{1+\varphi^2}} u_3^{[n]}(t)\right) \\
y^{[n+1]}(t) &= \frac{1}{n+1}\left(u_1^{[n]}(t) + u_2^{[n]}(t) - \frac{1}{\sqrt{1+\varphi^2}} u_3^{[n]}(t) + \mu u_5^{[n]}(t) - u_4^{[n]}(t)\right) \\
z^{[n+1]}(t) &= \frac{1}{n+1}\left(-\frac{\epsilon\varphi}{\sqrt{1+\varphi^2}} u_1^{[n]}(t) + \frac{\epsilon}{\sqrt{1+\varphi^2}} u_2^{[n]}(t) + (1-\varphi) u_3^{[n]}(t)\right)
\end{aligned} \tag{B.4}$$

The vectors $dx, dy, dz, dxp2$ and $dxdy$ store the values of $u_1^{[n]}(t), u_2^{[n]}(t), u_3^{[n]}(t), u_4^{[n]}(t)$ and $u_5^{[n]}(t)$ respectively. Once the normalized derivatives are computed, it just remains to choose an appropriate time step h (lines 143-166) to go from $x(t_k)$ to $x(t_{k+1}) = x(t_k + h)$. In our implementation of the Taylor method, we fix the order of the Taylor series to 24, and then we choose a value h such that the error between the actual solution x_{k+1} and the truncated solution at order 24 is of the order of the biggest term in the tail of the Taylor series (B.2). That is formally stated as:

$$\left| x^{[25]}(t_k) h^{25} \right|_\infty < tol \tag{B.5}$$

There, tol is defined as the product of a fixed small value and the maximum between the absolute value of the first normalized derivatives of each coordinate of x_k to make tol relatively small with respect to the sizes of the derivatives. From inequality (B.5), one obtains that:

$$h < \left(\frac{tol}{\left| x^{[25]}(t_k) \right|_\infty} \right)^{\frac{1}{25}}$$

To avoid cancellations caused, for example, by symmetries, we choose h taking into account the two last computed terms of the Taylor series, i.e., we take:

$$h = \min\left(\left(\frac{tol}{\left| x^{[24]}(t_k) \right|_\infty} \right)^{\frac{1}{24}}, \left(\frac{tol}{\left| x^{[23]}(t_k) \right|_\infty} \right)^{\frac{1}{23}} \right)$$

Notice that a new time step h is computed each time we call the *taylor* function. Once h is chosen and the normalized derivatives up to order 24 are computed, we can finally obtain the point x_{k+1} using equation (B.2). The sum is computed using the Horner's method (lines 171-178).

The Taylor method applied to the vector field $X_{\mu,\epsilon,-1}$ is easily implemented from the method applied to $X_{\mu,\epsilon,1}$. As seen in section 5.3.1, the vector field $X_{\mu,\epsilon,-1}$ describes the following system of differential equations:

$$X_{\mu,\epsilon,-1}(x,y,z) : \begin{cases} \dot{x} = y + (\varphi - 1)z \\ \dot{y} = x - y - z + \mu xy - x^2 \\ \dot{z} = \epsilon(1-\varphi)x + \epsilon y - \varphi z \end{cases}$$

This system presents very different dynamics compared to the system $X_{\mu,\epsilon,1}$, but its construction in section 5.1 was made that way so that the structure of the differential equations determining those systems remains similar. The only difference in the Taylor method is that now, in (B.4) one has that:

$$\begin{aligned} u_1^{[n]}(t) &= x^{[n]}(t) \\ u_2^{[n]}(t) &= y^{[n]}(t) \\ u_3^{[n]}(t) &= z^{[n]}(t) \\ u_4^{[n]}(t) &= \sum_{j=0}^{n} u_1^{[n-j]}(t) u_1^{[j]}(t) \\ u_5^{[n]}(t) &= \sum_{j=0}^{n} u_1^{[n-j]}(t) u_2^{[j]}(t) \\ x^{[n+1]}(t) &= \frac{1}{n+1}\left(u_2^{[n]}(t) + (\varphi - 1)u_3^{[n]}(t)\right) \\ y^{[n+1]}(t) &= \frac{1}{n+1}\left(u_1^{[n]}(t) - u_2^{[n]}(t) - u_3^{[n]}(t) + \mu u_5^{[n]}(t) - u_4^{[n]}(t)\right) \\ z^{[n+1]}(t) &= \frac{1}{n+1}\left(\epsilon(\varphi - 1)u_1^{[n]}(t) + \epsilon u_2^{[n]}(t) - \varphi u_3^{[n]}(t)\right) \end{aligned}$$

This can be carried on by modifying the lines 128, 129 and 130 in the code from section B.3.

B.3 Code in C

In this section, we show our code in C containing an implementation of the Taylor integration method. In [JZ05] one can find a software that works for a wide

variety of vector fields. Still, we decided to code our own program because we use a different step size control, and the algorithm is more efficient if it is made from scratch to find exclusively orbits of a predetermined vector field. The next code contains our implementation of the Taylor method applied to the vector field $X_{\mu,\epsilon,1}(x,y,z)$.

```
#include <stdio.h>
#include <stdlib.h>
#include <math.h>

double max3(double, double, double);
int taylor(double *, double *, double, double *, double, double, int, double,
    double, double);

int main (void) {
   int order, ind;
   double t, tmax, h, hmin, hmax, tol, mu, epsilon;
   double *x;
   char nameRes[25], nameData[25];
   FILE *results, *data;

   /* Initialize variables, allocate memory to the vectors and open files */
   order = 24;
   t = 0;
   tmax = 13;
   h = 0.1;
   tol = 1.e-16;
   hmin = 1.e-12;
   hmax = 0.01;
   ind = 0;

   x = (double *)malloc(3*sizeof(double));
   if(x == NULL) {
      printf("Memory error.\n");
      exit(1);
   }

   printf("Type the name of the file with the data.\n");
   scanf(" %s", nameData);
   data = fopen(nameData,"r");
   if(data == NULL) {
      printf("Error in the file %s\n", nameData);
      exit(1);
   }
   fscanf(data,"%le %le", &mu, &epsilon);
   fscanf(data,"%le %le %le", &x[0], &x[1], &x[2]);

   printf("Type the name of the file with the results.\n");
   scanf(" %s", nameRes);
   results = fopen(nameRes,"w");
   if(results == NULL) {
      printf("Error in the file %s\n", nameRes);
      exit(1);
   }
   fprintf(results,"%21.15le %21.15le %21.15le\n", x[0], x[1], x[2]);
```

```
49
50     /* Compute an orbit using Taylor's method */
51     while(ind == 0) {
52        ind = taylor(x,&t,tmax,&h,hmin,hmax,order,tol,mu,epsilon);
53        fprintf(results,"%21.15le␣%21.15le␣%21.15le\n", x[0], x[1], x[2]);
54     }
55
56     free(x);
57     fclose(results);
58     fclose(data);
59
60     return 0;
61 }
62
63
64 double max3(double a, double b, double c) {
65     double max = a;
66     if(b > max) {
67        max = b;
68     }
69     if(c > max) {
70        max = c;
71     }
72     return max;
73 }
74
75
76 int taylor(double *x, double *t, double tmax, double *h, double hmin, double
       hmax, int order, double tol, double mu, double epsilon) {
77     int diri, flag, iord, iop1, j, nj;
78     double phi, aux, aux1, aux2, h1, h2, relativeTol;
79     double *dx, *dy, *dz, *dxp2, *dxdy;
80
81     /* Allocate memory to the vectors */
82     dx = (double *)malloc((order + 1)*sizeof(double));
83     if(dx == NULL) {
84        printf("Memory␣error.\n");
85        exit(1);
86     }
87     dy = (double *)malloc((order + 1)*sizeof(double));
88     if(dy == NULL) {
89        printf("Memory␣error.\n");
90        exit(1);
91     }
92     dz = (double *)malloc((order + 1)*sizeof(double));
93     if(dz == NULL) {
94        printf("Memory␣error.\n");
95        exit(1);
96     }
97     dxp2 = (double *)malloc((order + 1)*sizeof(double));
98     if(dxp2 == NULL) {
99        printf("Memory␣error.\n");
100       exit(1);
101    }
102    dxdy = (double *)malloc((order + 1)*sizeof(double));
103    if(dxdy == NULL) {
```

```
104         printf("Memory error.\n");
105         exit(1);
106      }
107
108      /* Initialize the variables */
109      flag = 0;
110      phi = 0.5 * (1 + sqrt(5));
111      if((tmax - *t) > 0) {
112         diri = 1;
113      } else {
114         diri = -1;
115      }
116
117      /* Computation of the automatic derivatives */
118      /* Order 0 */
119      dx[0] = x[0];
120      dy[0] = x[1];
121      dz[0] = x[2];
122      dxp2[0] = x[0] * x[0];
123      dxdy[0] = x[0] * x[1];
124
125      /* Order >= 1 */
126      for(iord = 0; iord < order; iord++) {
127         iop1 = iord + 1;
128         dx[iop1] = (dy[iord] + (phi /(double)sqrt(1 + phi * phi)) * dz[iord]) /(
               double)iop1;
129         dy[iop1] = (dx[iord] + dy[iord] - (1 /(double)sqrt(1 + phi * phi)) * dz[
               iord] + mu * dxdy[iord] - dxp2[iord]) /(double)iop1;
130         dz[iop1] = (-((epsilon * phi) /(double)sqrt(1 + phi * phi)) * dx[iord] +
                (epsilon /(double)sqrt(1 + phi * phi)) * dy[iord] + (1 - phi) * dz[
               iord]) /(double)iop1;
131         aux1 = 0;
132         aux2 = 0;
133         for(j = 0; j <= iop1; j++) {
134            nj = iop1 - j;
135            aux1 += dx[nj] * dx[j];
136            aux2 += dx[nj] * dy[j];
137         }
138         dxp2[iop1] = aux1;
139         dxdy[iop1] = aux2;
140      }
141
142      /* Time step size control */
143      aux = max3(fabs(dx[1]),fabs(dy[1]),fabs(dz[1]));
144      aux1 = max3(fabs(dx[order-1]),fabs(dy[order-1]),fabs(dz[order-1]));
145      aux2 = max3(fabs(dx[order]),fabs(dy[order]),fabs(dz[order]));
146      relativeTol = tol * aux;
147      h1 = pow(relativeTol/(double)aux1,1/(double)(order-1));
148      h2 = pow(relativeTol/(double)aux2,1/(double)(order));
149      if(h1 < h2) {
150         *h = h1;
151      } else {
152         *h = h2;
153      }
154      /* Out of boundary cases and direction of time */
155      if(fabs(*h) > hmax) {
```

```
156         *h = hmax;
157     }
158     if(fabs(*h) < hmin) {
159         *h = hmin;
160     }
161     *h = diri * (*h);
162     /* Check that we did not escape tmax */
163     if(diri * (*t + *h) > diri * tmax) {
164         *h = tmax - *t;
165         flag = 1;
166     }
167     /* Update time */
168     (*t) = (*t) + (*h);
169 
170     /* Compute next point using Horner's method for the sum */
171     x[0] = dx[order];
172     x[1] = dy[order];
173     x[2] = dz[order];
174     for(j = order - 1; j >= 0; j--) {
175         x[0] = x[0] * (*h) + dx[j];
176         x[1] = x[1] * (*h) + dy[j];
177         x[2] = x[2] * (*h) + dz[j];
178     }
179 
180     free(dx);
181     free(dy);
182     free(dz);
183     free(dxp2);
184     free(dxdy);
185 
186     return flag;
187 }
```

Bibliography

[AKO14] Pablo Aguirre, Bernd Krauskopf, and Hinke M Osinga. Global invariant manifolds near a shilnikov homoclinic bifurcation. *Journal of Computational Dynamics*, 1(1):1, 2014.

[Ano67] Dmitry Victorovich Anosov. Geodesic flows on closed riemannian manifolds of negative curvature. *Trudy Matematicheskogo Instituta Imeni VA Steklova*, 90:3–210, 1967.

[Bel84] LA Belyakov. Bifurcation of systems with homoclinic curve of a saddle-focus with saddle quantity zero. *Mathematical Notes of the Academy of Sciences of the USSR*, 36(5):838–843, 1984.

[BF60] Friedrich L Bauer and Charles T Fike. Norms and exclusion theorems. *Numerische Mathematik*, 2(1):137–141, 1960.

[CKM86] LEONO Chua, Motomasa Komuro, and Takashi Matsumoto. The double scroll family. *IEEE transactions on circuits and systems*, 33(11):1072–1118, 1986.

[Fit61] Richard FitzHugh. Impulses and physiological states in theoretical models of nerve membrane. *Biophysical journal*, 1(6):445–466, 1961.

[GH13] John Guckenheimer and Philip Holmes. *Nonlinear oscillations, dynamical systems, and bifurcations of vector fields*, volume 42. Springer Science & Business Media, 2013.

[GL96] Paul Glendinning and Carlo Laing. A homoclinic hierarchy. *Physics Letters A*, 211(3):155–160, 1996.

[Gre15] Charlotte Greenblatt. An introduction to transversality. *Accessed online at http://schapos. people. uic. edu/MATH549_Fall2015_files*, page 1, 2015.

[HSD12] Morris W Hirsch, Stephen Smale, and Robert L Devaney. *Differential equations, dynamical systems, and an introduction to chaos*. Academic press, 2012.

[JZ05] Àngel Jorba and Maorong Zou. A software package for the numerical integration of odes by means of high-order taylor methods. *Experimental Mathematics*, 14(1):99–117, 2005.

[Kuz13] Yuri A Kuznetsov. *Elements of applied bifurcation theory*, volume 112. Springer Science & Business Media, 2013.

[Mos69] Jürgen Moser. On a theorem of anosov. *Journal of Differential Equations*, 5(3):411–440, 1969.

[Mos01] Jurgen Moser. *Stable and random motions in dynamical systems: With special emphasis on celestial mechanics*, volume 1. Princeton university press, 2001.

[NAY62] Jinichi Nagumo, Suguru Arimoto, and Shuji Yoshizawa. An active pulse transmission line simulating nerve axon. *Proceedings of the IRE*, 50(10):2061–2070, 1962.

[Pol] John C. Polking. Pplane 2005.10.

[Shi01] Leonid P Shil'nikov. *Methods of qualitative theory in nonlinear dynamics*, volume 5. World Scientific, 2001.

[Sot79] Jorge Sotomayor. *Li, cões de equa, cões diferenciais ordinárias*, volume 11. Instituto de Matemática Pura e Aplicada, CNPq, 1979.

[SS07] Leonid Pavlovich Shilnikov and Andrey Shilnikov. Shilnikov bifurcation. *Scholarpedia*, 2(8):1891, 2007.

[Tes12] Gerald Teschl. *Ordinary differential equations and dynamical systems*, volume 140. American Mathematical Soc., 2012.

[Wig13] Stephen Wiggins. *Global bifurcations and chaos: analytical methods*, volume 73. Springer Science & Business Media, 2013.